Warsaw University of Technology
Faculty of Physics

Tobiasz Czopowicz

Study of K^0_S meson production in NA61 experiment at the CERN SPS

Badanie procesów produkcji mezonów K^0_S w eksperymencie NA61 przy SPS w CERN

Master's Thesis

under supervision of Wiktor Peryt, Ph. D.

Warsaw, December 2010

Streszczenie

Jednym z głównych problemów, którymi obecnie zajmuje się fizyka zderzeń ciężkich jonów jest poszukiwanie plazmy kwarkowo-gluonowej (QGP), badanie jej właściwości oraz właściwości przejścia fazowego pomiędzy materią hadronową a QGP. Istnienie plazmy zostało po raz pierwszy zaproponowane w 1975 roku przez J. C. Collinsa and M. J. Perry'ego [1]. Wewnątrz plazmy kwarkowo-gluonowej kwarki oraz gluony, elementarne składniki materii, spodziewane są występować jako swobodne cząstki. W obserwowanym na co dzień świecie stan taki jest niemożliwy. Zawsze są uwięzione w hadronach.

Niestety plazmy kwarkowo-gluonowej nie można bezpośrednio zaobserwować eksperymentalnie. Istnieją jednak pewne zjawiska świadczące o jej istnieniu. Jest to między innymi wzmocnienie produkcji dziwności, tłumienie J/ψ, fluktuacje oraz tłumienie dżetów. Pozwalają one badać właściwości i zachowanie się plazmy.

W 2008 roku uruchomiony został największy akcelerator na świecie – LHC w CERN. Będzie on w stanie zderzać ze sobą protony przy energiach dochodzących do 14 TeV na parę nukleonów oraz jony ołowiu przy energii 5.5 TeV na parę nukleonów. Cztery duże i trzy mniejsze eksperymenty rozmieszczone przy akceleratorze badają najciekawsze obszary fizyki wysokich energii. Jednak z powodu zbyt wysokich energii, dane dotyczące QGP opisują obszar daleko poza przejściem fazowym.

Przeprowadzany przy akceleratorze SPS (Super Proton Synchrotron) w CERN eksperyment NA61/SHINE (SPS Heavy Ion and Neutrino Experiment), dzięki dużo niższej energii niż w eksperymentach przy LHC, koncentruje się na badaniach właściwości przejścia fazowego oraz przewidywanego punktu krytycznego. Pozwala to dostarczyć informacji na temat formowania się plazmy. NA61/SHINE zbada sygnatury QGP przy różnych dostępnych energiach oraz używając różnych rozmiarów pocisku i tarczy. Ponadto eksperyment zbiera dane referencyjne dla eksperymentów T2K (fizyka neutrin) oraz KASKADE-Grande (fizyka promieniowania kosmicznego).

Niniejsza praca magisterska poświęcona jest badaniu procesów produkcji mezonów K^0_S w zderzeniach wiązki protonów o pędzie 30.9 GeV/c z tarczą węglową. Dane zebrane zostały w 2007 roku przez eksperyment NA61/SHINE. Analiza została przeprowadzona w celu lepszego poznania mechanizmów produkcji cząstek dziwnych w zderzeniach przy niskich energiach SPS.

Abstract

One of the main problems of heavy-ion physics is search for the quark-gluon plasma (QGP), study its properties and characteristics of the phase transition between hadron nuclear matter and the QGP. Existence of the QGP has been introduced by J. C. Collins and M. J. Perry in 1975 [1]. In the QGP quarks and gluons, fundamental constituents of known matter, are expected to appear as free particles. Outside the plasma they are always confined inside hadrons.

Unfortunately the quark-gluon plasma can not be directly observed experimentally. However, there are certain phenomena that attest to its existence. These include strangeness production enhancement, suppression of J/ψ, fluctuations and jet quenching. They allow to study properties the plasma.

In 2008, the world's most powerful particle accelerator – the LHC at CERN has been launched. In the nearest future it will be able to collide protons at the energy of up to 14 TeV per nucleon pair and lead ions at the maximum energy of 5.5 TeV per nucleon pair. There are four big and three smaller experiments located at the accelerator exploring the most interesting areas of high energy physics. However, due to too high energy, data on the QGP describe the area beyond the onset of deconfinement.

NA61/SHINE (SPS Heavy Ion and Neutrino Experiment) operates at the SPS accelerator (Super Proton Synchrotron) at CERN with much less energy than in LHC. It focuses on the study of the phase transition and the expected critical point's properties. This would allow to provide information on the formation of the plasma. NA61/SHINE studies QGP signatures at different available energies and using different sizes of projectile and target. In addition, the experiment collects reference data for the T2K experiment (neutrino physics), and KASKADE-Grande experiment (cosmic ray physics).

This thesis is devoted to the study of production processes of K^0_S mesons in collisions of beam of protons with a carbon target at the beam momentum of 30.9 GeV/c. Data was collected in 2007 by the NA61/SHINE experiment. The goal of the analysis was to understand better mechanisms of production of strange particles in collisions at the low SPS energies.

Contents

Introduction **1**
Motivation . . . 1
Thesis' outline . . . 1
Author's contribution . . . 2

1 Heavy-ion physics **3**
1.1 The Standard Model . . . 3
1.1.1 Elementary particles . . . 3
1.1.2 Fundamental forces . . . 4
1.2 The Quark-Gluon Plasma . . . 5
1.2.1 QGP signatures . . . 6
1.3 High energy experiments . . . 7
1.3.1 Particle acceleration . . . 7
1.3.2 Particle detection and identification . . . 7
1.3.3 Experimental landscape . . . 9

2 K^0_S particle **11**
2.1 Properties . . . 11
2.2 Decay modes . . . 11

3 The NA61/SHINE experiment **13**
3.1 Physics programme . . . 13
3.1.1 Two dimensional phase diagram scan . . . 13
3.2 Experimental apparatus . . . 14
3.2.1 NA61/SHINE coordinate system . . . 15
3.2.2 Beam detectors . . . 15
3.2.3 Time Projection Chambers and magnets . . . 15
3.2.4 Time-of-Flight detectors . . . 16
3.2.5 Projectile Spectator Detector . . . 16
3.3 Gas System . . . 17
3.4 Readout and Data Acquisition System . . . 17
3.5 Detector Control System . . . 18

3.5.1 Old system 18

3.5.2 The upgrade 18

3.5.3 Plans for the future 19

4 NA61/SHINE offline software **21**

4.1 Reconstruction software 21

4.2 V^0 reconstruction 22

4.2.1 v0find 22

4.2.2 v0fit 23

4.3 Monte Carlo simulation 24

4.4 Data analysis tools 25

4.4.1 ROOT 25

4.4.2 ROOT61 25

5 Analysis **26**

5.1 Dataset selection 26

5.2 Events selection 26

5.2.1 BPD vertex cut 27

5.2.2 Fitted vertex existence cut 28

5.2.3 Fitted vertex quality cut 28

5.2.4 Fitted vertex z coordinate cut 28

5.2.5 Event cuts summary 29

5.3 All V^0 candidates 29

5.3.1 Invariant mass analysis 29

5.3.2 The Armenteros-Podolanski plot 30

5.4 V^0 selection 31

5.4.1 Invariant mass cut 31

5.4.2 Impact parameters cut 31

5.4.3 $\cos\theta^*$ cut 32

5.4.4 Δz cut 32

5.4.5 V^0 cuts summary 34

5.5 Binning 36

5.6 Uncorrected distributions 37

5.7 Efficiency and acceptance correction 38

5.8 Corrected distributions 39

5.9 Correction for inelastic events cut out 40

5.10 Normalization 40

6 Results and discussion **43**

6.1 Final K^0_S distributions 43

6.1.1 p_T and m_T distributions . . . 43
6.1.2 y* distribution . . . 44
6.2 Distributions' shapes . . . 44

Summary and conclusions **46**

List of Figures **47**

List of Tables **48**

Bibliography **49**

Introduction

Motivation

General aim of research in the field of ultrarelativistic heavy-ion physics is to study nuclear matter under conditions of extreme temperature and pressure. It should lead to the formation of a new state of matter, the Quark-Gluon Plasma, where quarks and gluons are deconfined – they exist as free particles [1]. It is believed that this state of matter have existed as one of the first after the Big Bang and possibly also exists in the cores of neutron stars.

It was predicted, that QGP can be created in the laboratory by colliding heavy nuclei at high energies. Such collisions have been studied over the last decades at energies increasing with technological progress – ability to build more powerful accelerators.

The experiment described in this thesis is performed at the European Organization for Nuclear Research (CERN) near Geneva, Switzerland.

Studying neutral kaons production is crucial for testing statistical models and for studying the "K to π" ratio.

Thesis' outline

The main goal of the analysis is to learn how to work with NA61/SHINE data and analysis methods by searching for K^0_S particles produced in the 2007 run period. Final results are the distributions of rapidity and transverse momentum.

First two chapters are the theoretical introduction. They are to outline the thesis' background of heavy-ion physics in general and K^0_S particles. Next chapter describes the NA61/SHINE experiment. Its physics goals and detectors. The experiment's offline software is presented in chapter 4 to explain how the data is transformed from raw ADC counts to events descriptions used for analysis. The procedure of searching for V^0s (i.e. K^0_S) is emphasized. Chapter 5 follows the analysis procedure step-by-step describing cuts, signal extraction and application of corrections. Results are presented in chapter 6, which also contains their discussion. Thesis ends with summary of what have been done and some ideas how to extend the analysis.

Author's contribution

The author, except for performing the analysis, contributes to the NA61 experiment as a member of the collaboration.

He takes an active part in meetings and international conferences (e.g. CPOD 2010). Also as a speaker. He is responsible for the Detector Control System, which plays a crucial role in running the experiment. He is also involved in creating completely new version of the system to suite NA61/SHINE needs and fully use available computing power and networking. He also contributed to the experiment's reconstruction software by making some fixes to the code.

Chapter 1

Heavy-ion physics

The main object of interest of high energy physics is the study of the structure of the matter, the subatomic particles. Heavy-ion physics combines nuclear physics, statistical physics, relativistic astrophysics and hydrodynamics to correctly describe the fundamental particles and forces.

1.1 The Standard Model

The Standard Model of Particle Physics is a quantum field theory describing elementary particles and their interactions. It explains most of high energy physics experimental data. It was developed throughout the early and middle 20th century and most of its predictions have been confirmed experimentally. The Standard Model fails to be a complete theory of fundamental interactions, though. It does not include gravity, it assumes neutrinos to be massless, quantitative predictions for strong interactions are limited to processes with a very large momentum transfer only and it has a large number of numerical free parameters.

1.1.1 Elementary particles

The Standard Model assumes existence of twelve elementary particles, which, together with their antiparticles, compose all known matter, and force carriers – bosons. These are six leptons (electron, muon, tau and their corresponding neutrinos) and six quarks (up – u, down – d, strange – s, charm – c, bottom – b and top – t). They are divided into three families. Summary of the particles' mass, electric charge (in electron charge units) and spin value is shown on figure 1.1. Quarks in the first family form the atomic nuclei in the universe. The four remaining quarks can create short-lived particles. Quarks compose hadrons. There are two groups of them. Particles, that consist of three quarks – baryons and those consisting of $q\bar{q}$ pairs – mesons. The latter are bosons (their spins have integer values), therefore they obey Bose-Einstein statistics. Leptons, quarks and baryons, having fractional spin values, are fermions and hence obey Fermi-Dirac statistics and

Pauli exclusion principle. Each quark can be in one of three color states (red, green or blue). Anti-quarks can be in one of three anti-color states (anti-red, anti-green or anti-blue). Three colors mixed together give a color-neutral charge. And only such particles are observed. While leptons exist as free particles, quarks do not. They are always confined in hadrons.

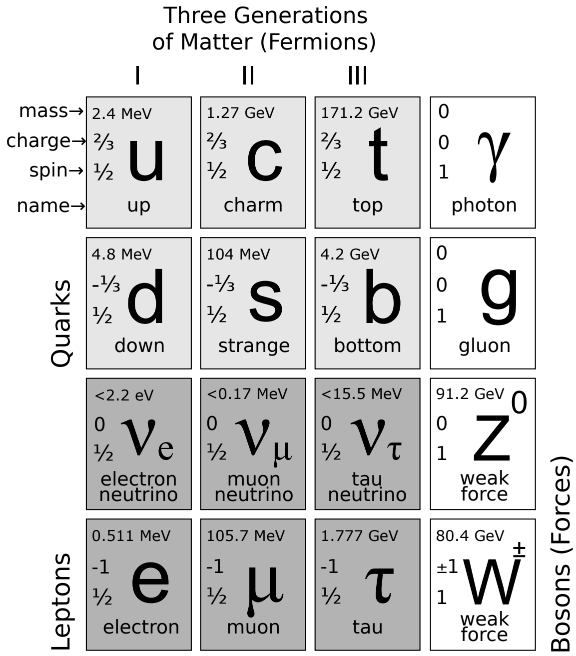

Figure 1.1: Elementary particles of the Standard Model.

1.1.2 Fundamental forces

The Standard Model explains three fundamental forces. These are strong, electromagnetic and weak. All forces require certain force carriers, which are exchanged between interacting particles. They are presented in figure 1.1. Strong nuclear force is responsible for the quark confinement. Its force carriers are eight gauge bosons - gluons. Strong interactions are described by Quantum Chromodynamics (QCD) – included in the Standard Model. Gluons, like quarks, carry the color charge, therefore the special feature of the force is the fact that its strength increases with distance.

Electromagnetic force is 100 times weaker than the strong force. It affects all charged particles. Photons are its force carriers. The force is described by Quantum Electrodynamics (QED).

Weak nuclear force affects all leptons, quarks and neutrinos. Its force carriers are heavy gauge bosons – W and Z. The weak interaction is the only one that violates P and CP symmetries and changes particles' flavor. It is 10^{13} times weaker than the strong force. The weak and electromagnetic forces have been successfully unified to electroweak interactions.

Standard Model includes also the Higgs boson. It is a hypothetical elementary particle, that would be responsible for other particles' masses. The existence of the particle is postulated as a means of resolving inconsistencies in the Standard Model. Attempts are being made to confirm the existence of the particle by the LHC experiments.

Table 1.1: Summary of fundamental forces of the Standard Model.

Interaction	Theory	Force carrier	Relative strength	Range [m]
Strong	QCD	gluon	10^{38}	10^{-15}
Electromagnetic	QED, Electroweak	photon	10^{36}	∞
Weak	Fermi coupling, Electroweak	W and Z bosons	10^{25}	10^{-18}
Gravitation	General Relativity	graviton (hypotetical)	1	∞

1.2 The Quark-Gluon Plasma

The Quark-Gluon Plasma (QGP) is a state of matter, when quarks and gluons are deconfined. QGP requires either extremely high energy density. Quarks are no longer trapped inside hadrons, but “swim” freely in a “quark soup”. After approximately 10^{-23} second, as QGP expands, energy density decreases and quarks become confined and compose hadrons. It is believed, that QGP was one of early stages of evolution of the universe. It is possible to go back in time and learn about the Big Bang by studying it. QGP may also appear inside neutron stars.

The QGP can be created by raising energy density to approximately 1 GeV/fm^3. This can be accomplished by colliding two heavy nuclei accelerated to high energy. Figure 1.2 shows a theoretical phase diagram of strongly interacting matter with Hadron Gas and QGP states as well as predicted critical point and first order phase transition line marked.

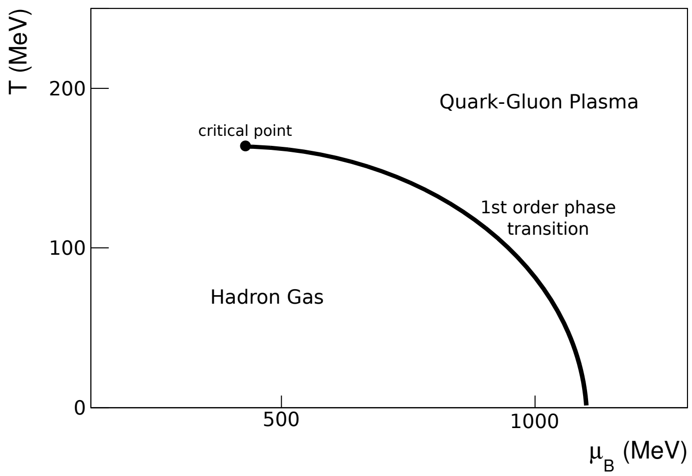

Figure 1.2: Theoretical phase diagram of strongly interacting matter.

1.2.1 QGP signatures

Only hadrons can be observed in experiments. But some evidences of QGP existence have been theoretically predicted [2]. They have been observed in lead and gold nuclei collisions at CERN and Brookhaven National Laboratory, USA.

Charmonium suppression

The heavy charm pair (c and $\bar{c}$ quarks – components of for example J/ψ meson) production takes place very early. Its production would be suppressed with respect to the nucleon-nucleon collisions [3]. The deconfining environment of the Quark-Gluon Plasma prohibits the formation of $c\bar{c}$ bound states. The Debye screening of the QGP reduces production of a J/ψ state in heavy ion collisions, and the low temperatures at the hadronization do not permit production of $c\bar{c}$ pair kinematically.

Electromagnetic signals

Particles which do not interact strongly (leptons, photons), are unaffected by the process of hadronization. Those of them, which are produced in QGP deliver information from the phase where they were created, in the form of production rates and momentum distributions.

Jet quenching

In heavy-ion collisions hadron jets – narrow cone of hadrons and other particles – are often produced. They are created by hadronization of a high transverse momentum quark. Jets should be produced as oppositely directed pairs. If one of them is missing, than it is interpreted, that it has been absorbed by the QGP. Indeed such effect was observed by RHIC experiments [4].

Strangeness enhancement

In proton-proton collisions the production of particles containing a strange quark or anti-quark is strongly suppressed compared to the production of particles containing only u and d quarks. This is explained by the higher mass of the s quark. Energy needed to produce strange quarks inside QGP is more than two times smaller than in the hadron gas. That is why strangeness enhancement in nucleus-nucleus collisions should be observed [5].

Fluctuations

Large fluctuations in certain observables are expected at the QCD phase transition as in the phase transition region various phenomena development is enhanced. It is possible to search for these event-by-event fluctuations [6, 7] by looking for non-statistical deviations in distributions of events when compared to the ones constructed by mixing particles from different events.

1.3 High energy experiments

The only way to validate theoretical predictions is to set up an experiment. High energy physics requires big and expensive facilities and involves work of many people. Nevertheless there are a few experiments aimed to discover the QGP and study its properties.

1.3.1 Particle acceleration

Before beam particles interact with the target, they have to be accelerated to required energies. There are many accelerators in different scientific institutions around the world. Basis for their operation if the fact, that when a charged (q) particle passes through electric E and magnetic B fields, it changes its direction and velocity v due to Lorentz force:

$$\vec{F} = q\vec{E} + q\vec{v} \times \vec{B}.$$

The first component allows to build linear accelerators, where particles are exposed to increasing electric field. Second component allows to bend particles trajectory and, by changing the magnetic field, maintain a constant bend radius. This is the main idea of a synchrotron.

One of the oldest working synchrotron is the SPS (**S**uper **P**roton **S**ynchrotron). It is a 6.9 km long particle accelerator at CERN. It has been used to accelerate protons, anti-protons, electrons, positrons and heavy ions up to 450 GeV per nucleon since 1967. SPS is also being used by the CNGS experiment to produce a neutrino stream to be detected at the Gran Sasso laboratory, Italy, 730 km from CERN. SPS is not a collider. It provides hadron beams for fixed-target experiments.

Another synchrotron is RHIC (**R**elativistic **H**eavy-**I**on **C**ollider). It is located at Brookhaven National Laboratory in USA. It has been operating since 2000. The RHIC ring is hexagonally shaped and 3.8 km long in circumference. It is capable of colliding gold ions from 7.7 to 200 GeV per nucleon pair, protons up to 500 GeV, and asymmetric systems like deuterons with heavy nuclei.

The newest synchrotron is the LHC (**L**arge **H**adron **C**ollider). It is the world's largest and highest-energy particle accelerator. It lies in a 27 km circumference tunnel. This synchrotron is designed to collide protons beams injected from SPS at 450 GeV and then accelerated up to 7 TeV per particle. It is also capable of accelerating lead ions to 5.5 TeV per nucleon pair.

1.3.2 Particle detection and identification

Particles produced in the collision have to be detected and identified. One of the most popular detector type widely used in high energy experiments is a Time Projection Chamber (TPC). It is a chamber filled with gas. At one side the gas volume is limited by the high voltage plane and at the other – readout plane. It is a metal plane segmented into small pieces – pads. Three grids of wires are spanned parallel to the readout plane: the field wire grid, the sense wire grid, the frisch-grid and the gating-grid (fig 1.3).

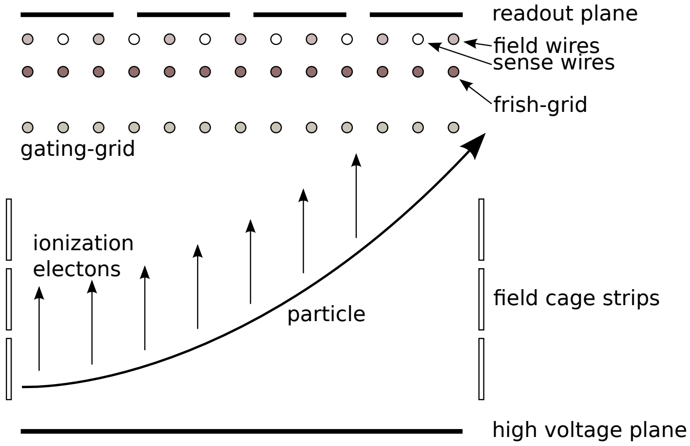

Figure 1.3: Time Projection Chamber scheme.

A charged particle passing through the gas inside the TPC interacts with its atoms, and ionizes. Then, produced electrons begin to drift towards the readout plane, due to the almost homogenous electric field between the high-voltage plane and the frisch-grid. This region is called the drift region. The strength of this electric field is tuned such that no avalanche effect takes place in the drift region.

All drift electrons, arriving from the drift region through the frisch-grid, are collected on the sense wires. The electric field between the frisch-grid and the sense wires is bigger than that in the drift region. In addition, the electrons are further accelerated close to the sense wires, and produce an avalanche. The electrons are collected and removed by the sense wires, and the remaining positive ions produce an induced signal in the pads of the readout plane. Each pad is read out separately and the projection of the particles' trajectories onto the readout plane are known. The third coordinate of the points on the trajectories is determined by measuring the drift velocity of the electrons. After fitting particles' trajectories to the ionization points, its momentum can be calculated by studying their bend due to the presence of the magnetic field.

One of the methods of identification is measuring the energy loss (dE) inside the TPC. Charged particles traveling through a medium looses energy as described by the Bethe-Bloch formula:

$$-\frac{dE}{dx} = \frac{e^2 Z^2 n_e}{4\pi\epsilon_0^2 m_e c^2 \beta^2}\left[ln\frac{2m_e c^2 \beta^2 \gamma^2}{I\left(1-\beta^2\right)} - \beta^2\right],$$

where m_e and e are the electron's mass and charge, Z is the charge of the particle and n_e and I are the number of electrons per unit volume and the average ionization energy of the material. Protons, pions, kaons and electrons exhibit different characteristic specific energy loss curves as a function of momentum.

Another method is to use a Time-of-Flight (ToF) detector. It is able to discriminate between a lighter and a heavier elementary particle of same momentum using their time of flight between two scintillators.

If the measurement of the energy loss, momentum and mass are done independently, then particles can be identified. Figure 1.4 shows how the identification is done.

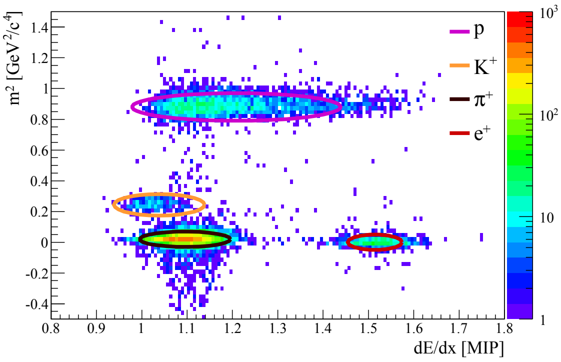

Figure 1.4: $\frac{dE}{dx}$ vs ToF for 1–2 GeV/c particles (NA61/SHINE).

Neutral particles are identified only by their decay topology as they do not ionize gas inside TPCs. Also, their trajectories do not bend in magnetic field.

1.3.3 Experimental landscape

Heavy-ion physics: NA49

NA49 [8] was a fixed target experiment designed to study heavy-ion collisions using p+p, C+C, Si+Si and Pb+Pb interactions at center of mass energy $\sqrt{s_{NN}} = 6.3 - 17.3$ GeV at the CERN SPS. Data taking started in 1994. The experiment finished operating in 2002. NA49 successor is the NA61 experiment.

Heavy-ion physics: STAR

STAR (**S**olenoidal **T**racker **A**t **R**HIC), is one of detectors at RHIC. The primary physics tasks of the experiment is to study the formation and characteristics of QGP [9] and the origin of spin in protons. In 2010 STAR started the Beam Energy Scan for studying the phase diagram of strongly interacting matter. The collaboration consists of over 600 scientists and engineers from over 55 institutions in 12 countries.

Heavy-ion physics: ALICE

ALICE (**A** **L**arge **I**on **C**ollider **E**xperiment) is a general purpose heavy-ion experiment designed to study physics of strongly interacting matter and the Quark-Gluon Plasma in nucleus-nucleus collisions at the CERN LHC. The experiment will perform collisions of lead as well as lighter ions to study the system under different energy densities. Also proton-proton and proton-nuclei data will be collected, which will provide reference data for the nucleus-nucleus collisions and allow for a number of p+p physics studies. The ALICE collaboration consists of more than 1000 scientists from 105 institutes in 30 countries.

Neutrino physics: T2K

The T2K (**T**okai **to** **K**amioka) experiment [10] is the next generation (K2K experiment successor) long baseline neutrino oscillation experiment in Japan. A 50 GeV muon neutrino beam is produced at the J-PARC accelerator center in Tokai and is sent 295 km to be detected by the Super-Kamiokande detector in Kamioka.

The precise measurement of the neutrino oscillation is one of the keys to reveal the origin of mass. Therefore the goals of the experiment at the first stage are:

- discovery of $\nu_\mu \rightarrow \nu_\mathrm{e}$ oscillation,
- precise measurement of the oscillation parameters in ν_μ disappearance,
- measurement of the neutral current events in search for a sterile component in ν_μ disappearance.

After these goals are successfully achieved, CP violation in the lepton sector will be measured with the upgraded, 5 times more powerful, accelerator and with the Hyper-Kamiokande detector (20 times larger than the current one).

Cosmic-ray physics: KASCADE-Grande

KASCADE-Grande (**Ka**rlsruhe **S**hower **C**ore and **A**rray **De**tector - **Grande**) [12] is a multi-detector experiment for the measurement of air showers induced by primary cosmic rays in the energy range $10^{16} - 10^{18}$ eV. It is a successor of the KASCADE experiment, which aim was to investigate the cosmic ray flux in a specific region of the cosmic-ray spectrum ("knee region"). KASCADE-Grande consists of an array of 37 scintillator stations for measuring the electromagnetic component of air showers. The muonic component is measured with the detectors of KASCADE by scintillation counters and tracking chambers at different particle energy thresholds.

Chapter 2

K^0_S particle

A neutral kaon (K^0) was first recorded in 1947 in one of two cloud chamber's photos illustrating events induced by cosmic-ray particles. There was a neutral particle decaying into two charged pions. Its mass was estimated to be about half the mass of proton. Later a new quantum number called "strangeness" was introduced. It is conserved in strong, but violated in weak interactions.

2.1 Properties

Neutral kaons are mesons – they consist of a $q\bar{q}$ pair. K^0 consists of d and $\bar{s}$ quarks and $\bar{K}^0$ – $\bar{d}$ and s. K^0 have two weak eigenstates: K^0_S (short-lived) and K^0_L (long-lived):

$$\left|K^0_S\right\rangle = \frac{1}{\sqrt{2}}\left(\left|K^0\right\rangle + \left|\bar{K}^0\right\rangle\right)$$

$$\left|K^0_L\right\rangle = \frac{1}{\sqrt{2}}\left(\left|K^0\right\rangle - \left|\bar{K}^0\right\rangle\right)$$

K^0_S mass is $m = 0.498$ GeV/c^2, its mean life $\tau = 0.90 \times 10^{-10}$ s, which gives $c\tau = 2.68$ cm [13].

2.2 Decay modes

Decay modes of K^0_S are listed in table 2.1. The most probable is a decay into two oppositely charged pions hence most neutral kaons decay in this mode. This fact is very convenient from the experimental point of view as both daughter particles carry charge and can be easily registered and identified with Time Projection Chamber detectors with magnetic field.

Table 2.1: K^0_S decay modes [13].

mode	fraction $\left(\frac{\Gamma_i}{\Gamma}\right)$
$K^0_S \to \pi^+\pi^-$	(69.20 ± 0.05) %
$K^0_S \to \pi^0\pi^0$	(30.69 ± 0.05) %
$K^0_S \to \pi^+\pi^-\pi^0$	$3.5^{+1.1}_{-0.9} \times 10^{-7}$

Chapter 3

The NA61/SHINE experiment

NA61/SHINE (**S**PS **H**eavy **I**on and **N**eutrino **E**xperiment) [14, 15] is a fixed-target experiment located in the North Area of the Super Proton Synchrotron (SPS) accelerator facility at the European Organization for Nuclear Research (CERN) in Geneva, Switzerland. It is a successor of the NA49 experiment, which was operating in 1994 – 2002.
The NA61 collaboration consists of 130 physicists from 24 institutes in 13 countries.

3.1 Physics programme

The experiment measures hadron production in proton-proton, proton-nucleus and nucleus-nucleus collisions. After the first technical run in August 2006, when all detectors inherited from NA49 were tested, first physics data were collected in October 2007 for pilot analysis. The experiment is planned to run for five years and finish in 2014 collecting over 200 million events.

NA61/SHINE physics goals are:

- search for the critical point of strongly interacting matter,
- detailed study of the onset of deconfinement,
- study of the suppression of high p_T hadrons in p+p and p+Pb interactions,
- reference measurements for the T2K (section 1.3.3) experiment by measuring the neutrino fluxes from the T2K beam targets in p+C collisions [16, 17],
- reference measurements for cosmic-ray physics (section 1.3.3) by measuring p+C, π^++C and π^-+C interactions [18, 19].

3.1.1 Two dimensional phase diagram scan

In order to search for the critical point and study the properties of the onset of deconfinement, NA61/SHINE will perform a 2D phase diagram scan. It will measure hadron production in various energies (13A, 20A, 30A, 40A, 80A and 158A GeV) in various collisions (p+p, p+Pb, B+C, Ar+Ca, Xe+La) [20]. Collected data, together with Pb+Pb reactions recorded by NA49 would allow to cover the region, where the critical point is expected. According to lattice calculations T $= 162 \pm 2$ MeV and $\mu_{\mathrm{B}} = 360 \pm 40$ MeV [21].

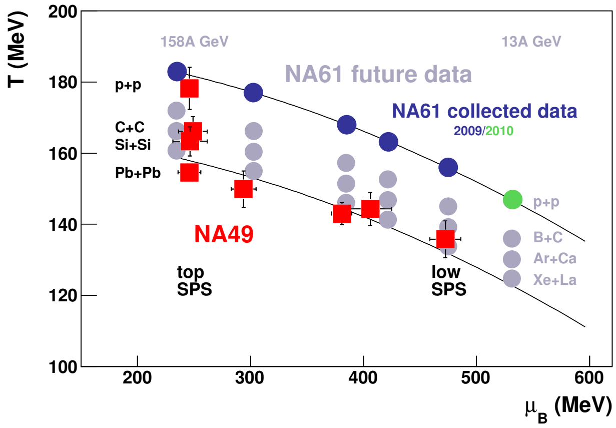

Figure 3.1: Theoretical phase diagram region explored by NA61/SHINE and NA49.

3.2 Experimental apparatus

NA61/SHINE is a large acceptance hadron spectrometer. The main components of the current detector were constructed and successfully used by the NA49 [22]. Experimental set-up is shown in figure 3.2.

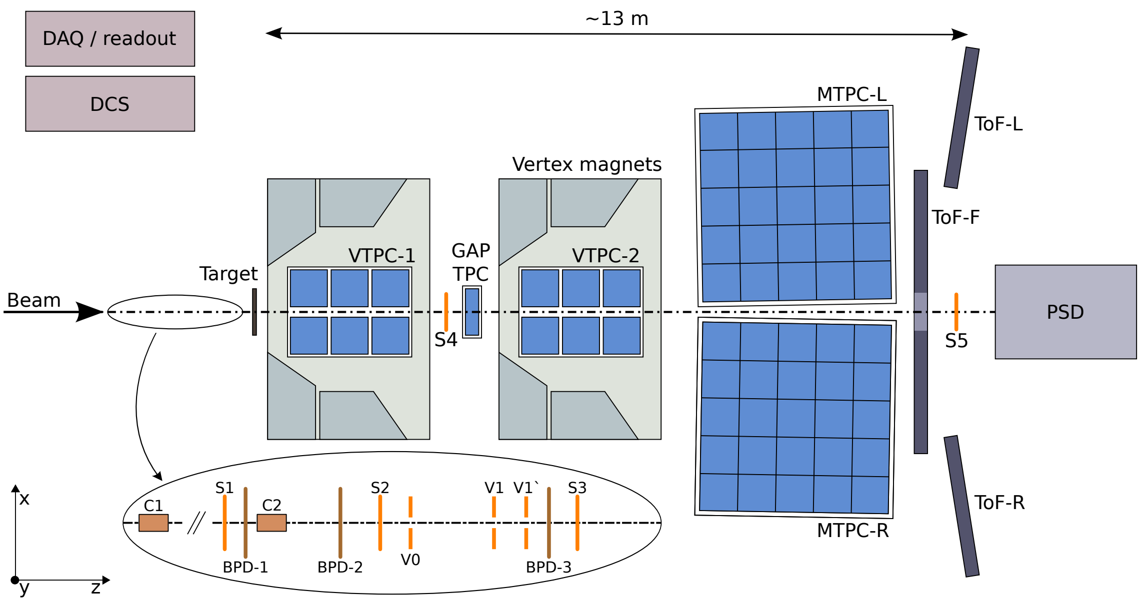

Figure 3.2: The layout of NA61/SHINE experimental set-up top view (not to scale).

3.2.1 NA61/SHINE coordinate system

In the NA61/SHINE coordinate system z axis is defined by the beam direction, y points upwards and x horizontal and positive to the left (as looking downstream the beam). For historical reason, the origin of these coordinates is located in the center of VTPC-2. Therefore the target is located at z = -580 cm.

3.2.2 Beam detectors

Transverse positions of the beam are given by three Beam Position Detectors (BPD-1/2/3). They are 48 × 48 mm^2 proportional chambers filled with Ar/CO_2 gas mixture with a cathode strip readout (32 strips with 1.5 mm pitch). Each detector consists of two orthogonal wire (15 μm thick tungsten) planes sandwiched between three cathode planes made of 25 μm aluminized Mylar.

There is also a set of scintillators, which signals' combination is used to trigger data acquisition and to provide precise timing information. S1, S2, S3, V0, V1 and V1' are mounted in the beam line before the target, whereas S4 and S5 are installed downstream. There are also two Čerenkov counters (C1 and C2) to select desired particles from the secondary hadron beam.

The individual beam particle position measured in these detectors allows for reconstruction of the interaction point in the target with a precision of 40 μm for proton and 170 μm for lead beams.

3.2.3 Time Projection Chambers and magnets

The main tracking devices are four large volume Time Projection Chambers (TPC) inherited from NA49. Two of them ("vertex" TPCs: VTPC-1 and VTPC-2) are located in the magnetic field, two others ("main" TPCs: MTPC-L and MTPC-R) are positioned downstream of the magnets symmetrically to the beam line. There is also a smaller TPC (GAP TPC) constructed at the end of NA49 operating period. It is mounted between two VTPCs, centered on the beam line for measuring particles with the smallest production angles.

Dimensions of the TPCs are presented in table 3.1.

Table 3.1: Dimensions of NA61/SHINE TPC detectors.

dimension [mm]	VTPC-1/2	MTPC-L/R
x (perpendicular to beam line)	2000	3900
y (height)	980	1800
z (parallel to beam line)	2500	3900
drift length	666	1117

Typical TPC resolution varies from $\frac{\sigma_p}{p^2} = 7.0 \times 10^{-4}$ (GeV/c)$^{-1}$ for tracks detected in VTPC-1 only, down to $\frac{\sigma_p}{p^2} = 0.3 \times 10^{-4}$ (GeV/c)$^{-1}$ for tracks detected in VTPC-2 and one of the MTPCs. These detectors allow reconstruction of over 1000 tracks in one Pb+Pb interaction.

Thanks to their size, MTPCs allow also for the measurement of energy loss in gas ($\frac{dE}{dx}$). It is possible to register up to 90 samples of energy loss per track providing high statistics for precise measurement.

VTPCs are located inside two superconducting dipole magnets to enable measurements of charged particles' momenta based on their tracks' bending. The magnetic field is parallel to the electric field so that it does not affect the drift direction. The field for 158A GeV beam energy is 1.5 T in the upstream magnet (VTPC-1) and 1.1 T in the downstream magnet (VTPC-2). It is reduced for lower beam energy.

3.2.4 Time-of-Flight detectors

Two Time-of-Flight (ToF-L/R) detectors were introduced in NA49 to improve particle identification at low ionization. They are comprised of two arrays, consisting of 891 scintillators and covering area of 2 × 1.2 m^2 each. Overall time resolution is $\sigma_{\mathrm{ToF-L/R}} \approx 60$ ps.

In order to extend the acceptance of NA61/SHINE to satisfy T2K needs, a new forward detector (ToF-F) was constructed. It is placed between side ToFs, just behind MTPCs. It consists of 64 scintillator bars with read-out on both sides, has total area of 5.77 × 1.2 m^2 and time resolution of $\sigma_{\mathrm{ToF-F}} \approx 120$ ps.

3.2.5 Projectile Spectator Detector

The most downstream detector is the Projectile Spectator Detector (PSD). It was designed to measure number of non interacting nucleons from a projectile nuclei on event-by-event basis. These quantities allow to determine the centrality of the collision.

PSD consists of 20 small (10 × 10 cm^2) and 20 large (20 × 20 cm^2) modules, each 120 cm long. Whole detector weights about 17 tons. Each module consists of 60 consecutive lead (16 mm) and scintillator (4 mm) layers sandwiched perpendicular to the beam.

Detector's resolution for measurement of the total energy of the projectile spectators is $\frac{\sigma_E}{E} < \frac{50\%}{\sqrt{E}}$ in a very broad energy range from 10 GeV to 30 TeV, which should lead to a low uncertainty in the determination of the number of interacting nucleons even for peripheral collisions of heavy nuclei at low energies.

Also, a high granularity of the energy measurement, which will enable the separation of contributions of different particles (protons, neutrons, nuclei fragments).

3.3 Gas System

The detector gas is supplied by four independent gas systems. Each system recirculates the gas with a compressor at a rate of about 20% detector volume per hour (0.6 and 4.0 m^3/h for VTPCs and MTPCs, respectively). Flow control is achieved by regulating the TPC over-pressure to 0.50 ± 0.01 mbar via frequency modulation of the recirculation pumps.

Fresh gas is mixed and fed into the system through mass flow controllers. In normal operation, the fresh gas is supplied at only 2% detector volume per hour. Oxygen is cleaned from the detector gas by filter columns containing active Cu granules chosen for use with the CO_2 gas mixtures. Fresh filters absorb water contamination in the gas over periods of some weeks, such that the water content may vary by 10 to 20 ppm.

The required $\frac{\mathrm{dE}}{\mathrm{dx}}$ performance and space resolution in drift direction force gas mixtures to be stabilized to a very high level of accuracy. Gas purities of $2 - 4$ ppm oxygen and about 20 ppm water are typically achieved.

Each of the gas systems has a system of four gas amplitude monitors and one drift velocity monitor. The amplitude monitors measure the signal from ^{55}Fe photons in a proportional tube, both in the fresh gas input line and in the recirculated gas. Pressure and temperature variations are corrected. Drift velocity is measured in a drift detector using the drift time difference from a pair of α sources at 10 cm distance.

3.4 Readout and Data Acquisition System

The most important software system of the experiment is Data Acquisition (DAQ). It is responsible for collecting data from all detectors, performing basic processing and sending it to the experiment's storage disk space. It has been completely rewritten since NA49 to operate with the new read-out electronics. These changes made it possible to record up to 80 events per second. The NA61 TPC read-out system has three main components:

- Motherboards that organize the read-out of front-end cards and build the data structure. It also performs pedestal subtraction, threshold comparison, zero suppression and Huffman coding. A motherboard is able to read-out data from 24 cards in parallel.
- Concentrator Boxes that are stand-alone boxes with 32 bidirectional LVDS inputs/outputs. A maximum of 32 motherboards can be connected to one concentrator box. During the read-out, the concentrator de-serializes the incoming data streams and multiplexes them into a single 32-bit wide data stream. Then the 32-bit data flow is transmitted to the server PCs through DDL links. In the other directions, the concentrator receives commands, pedestal and other data from the DAQ computers addressed to the motherboards. The concentrator will route the data to the appropriate motherboard.

- Detector Data Link (DDL) which are high-speed, serial optical links with parallel interfaces developed for the ALICE experiment. DDL transfers detector data to the DAQ computer with minimum rate of 200 MB/s, and data blocks and commands from the data acquisition system via the backward channel with a minimum rate of 10 MB/s.

3.5 Detector Control System

Another software system, crucial to run the experiment, is the Detector Control System (DCS). It's main tasks are:

- to control and monitor low voltages applied to TPC readout electronics,
- to control and monitor high voltages applied to various detectors,
- to control and monitor gas system parameters, in particular drift velocity, which is essential for data reconstruction procedure,
- to monitor various detector and atmospheric parameters (temperatures, pressure, humidity, magnetic field, etc.).

3.5.1 Old system

The old DCS was designed in mid 90's for NA49. It was running under MAC OS-9 operating system using LabVIEW programming environment (version 3.0). It consisted of four standalone applications: Low Voltages control, High Voltages and Trigger control, Gas System control and Beam Position Detectors monitoring.

The system was found to be unreliable and out-dated by the NA61/SHINE collaboration. As more computing power and disk space was available and hardware upgrades were planned, a decision was made to design a completely new system.

3.5.2 The upgrade

Before 2007 run all applications were moved in two steps to LabVIEW 8.5 and to Linux operating system (Debian 5). Because of hardware upgrades, communication with new VME (CAEN V2718 with A2818 PCI card) and CAMAC (CAEN C111C) controllers had to be written. After 2007 run a new high voltages power supply communication (via CAEN PCI card A1303) was implemented. Because of increase of complexity, trigger control application was separated from high voltages control application. Some new functionality (e.g. radioactivity measurement) were introduced to all the applications. Before 2009 run first steps were taken to rewrite LabVIEW applications to C (pressure and drift velocity measurements were rewritten).

3.5.3 Plans for the future

Since 2007 actions have been taken to completely rewrite the whole DCS. Schema of the new system is shown in figure 3.3.

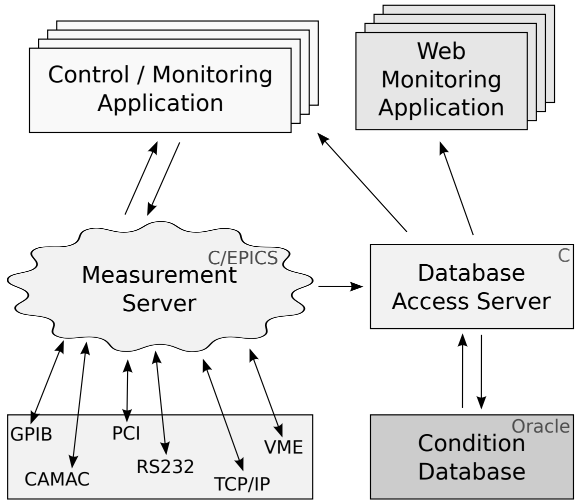

Figure 3.3: NA61/SHINE new DCS schema.

The heart of the system will be the Measurement Server. It will be written in C programming language using EIPCS (Experimental Physics and Industrial and Control System) [23] toolkit, which is a set of Open Source libraries and software tools used all over the world to create distributed real-time control systems.

The Server will run as a background process performing all necessary measurements and sending all results to the Condition Database through the Database Access Server. It will be accessible for experts only.

The Condition Database will store all measurements' results. It will be an Oracle database maintained externally by the CERN IT division.

The Database Access Server will manage all connections to the Condition Database. This is the only way (for non-experts) to retrieve data from the database.

Control/monitoring applications will be written in C programming language using GTK+ libraries. They will enable control and monitoring of the Measurement Server and display data from the Condition Database for DCS operators.

Web monitoring applications as a part of NA61/SHINE's website will display measurements' results from the Condition Database.

By rewriting the whole system not only better support for new hardware will be achieved but also performance and reliability will improve. The main advantages of this new system compared to the old one are:

- separating measurements from visualization – displaying results does not influence measurements,

- storing results in a proper database instead of plain text files or LabVIEW special binary files (readable for LabVIEW only) – standardized way of keeping data available for many applications,
- web monitoring allows NA61 collaborators to monitor the system's activities and measurements' results from all over the world,
- the Measurement Server can be controlled and monitored remotely (by experts only) from all over the world.

New system is expected to be introduced in 2011 run.

Chapter 4

NA61/SHINE offline software

Each modern experiment, weather physics or not, could not operate without computers. NA61/SHINE is no exception. Huge amounts of collected data need to be stored, processed and analyzed. It could not be done without computer software.

4.1 Reconstruction software

There is a long way from raw data (signals collected from all detectors – ADC counts) to complete events' information ready to use for physicists (fig. 4.1). That makes NA61/SHINE reconstruction software crucial for any analysis. Heart of the software is the DSPACK server [24]. It serves data for client applications. They are run in chain retrieving necessary data, performing various operations and sending processed data back for use by other clients. Order of running and function of clients is shown in table 4.1. There are also few not listed so-called miniclients, that perform smaller but also very important tasks (e.g. applying drift velocity corrections).

After all clients are run, reconstructed events are stored as objects (C structures) in a DST (Data Summary Tape) format. DST files can be then converted into ROOT mini-DST files using ROOT61 framework. Only data essential for the analysis is copied. Typical raw data file is about 1 GB, DST file – 350 MB, whereas ROOT mini-DST is only about 1 MB.

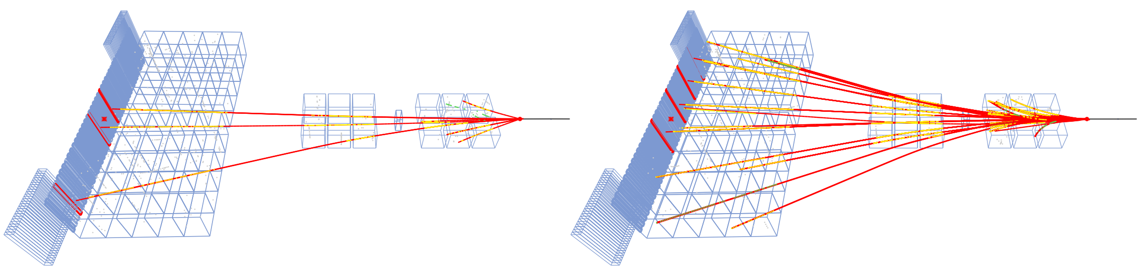

Figure 4.1: Samples of reconstructed events: p+C at 30.9A GeV (left) and π^-+C at 158A GeV (right).

Table 4.1: Event reconstruction chain procedure.

client	action
`dipt`	Charge clusters (points) are found in all TPCs.
`tpc_res_corb`	Electric and magnetic field distortions are corrected.
`mtrac`	Straight tracks are reconstructed in MTPCs.
`mpat`	MTPC tracks are extrapolated to VTPCs.
`patrec`, `r3d`	Tracks in VTPCs not extrapolated from MTPCs are matched and fitted.
`mpat`, `r3d`	Global tracks are matched, refitted and have momentum assigned.
`vtx`	The main vertex is located from a fit of global tracks.
`domerge`	Split global tracks are identified, merged and refitted.
`v0find`	V^0s are reconstructed using global tracks.
`v0fit`	Reconstructed V^0s are geometrically fitted.
`xi_find`	Cascades and Ωs are reconstructed from V^0s and global tracks.

4.2 V^0 reconstruction

For the analysis of this thesis, `v0find` and `v0fit` clients are of particular importance. They are run almost at the end of the reconstruction procedure, when all tracks are reconstructed and all momenta are calculated. Their task is to find and fit particles, which decay into a positive and a negative daughter leaving a track, that looks like a letter "V". "^{0}" means that these particles are neutral – they do not ionize inside TPCs, and hence do not leave tracks. Possible candidates for V^0s are K^0_S, Λ and $\bar{\Lambda}$.

4.2.1 v0find

First client application, `v0find`, loops through all positive tracks and tries to match a negative one. There are certain conditions that these two tracks have to meet to be considered as V^0 daughters (fig. 4.3).

- Both tracks have to leave sufficient number of points inside TPCs. It ensures, that tracks are properly fitted by `r3d` client.
- Extrapolated tracks have to be close enough to each other at some point. This distance is called the Distance of Closest Approach (DCA) and is measured along x and y axis. However, DCA is only calculated if extrapolated V^0 candidate's z coordinate value is greater than z_{V^0}.
- Extrapolated tracks are required to have a certain separation at the target plane in x and y direction ("x1minx2", "y1miny2").
- Extrapolated V^0 candidate have to be close enough to the target (x and y coordinates at the target plane – "xtv0", "ytv0").
- Angle (ϕ) between the normal to the decay plane and the vector y that is perpendicular to

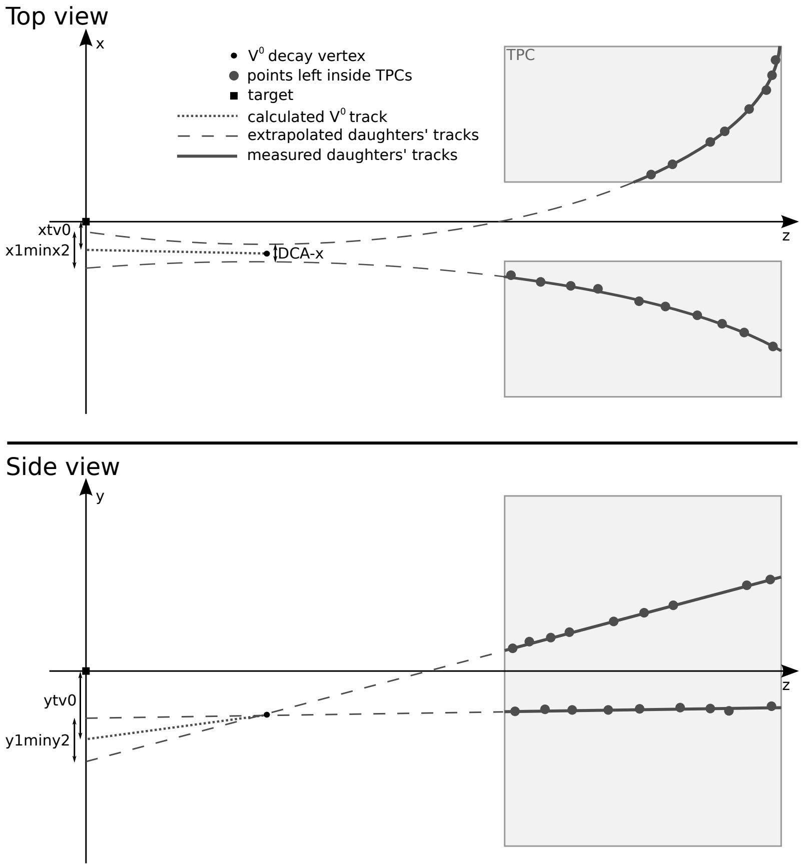

Figure 4.2: Graphical explanation of cuts used by `v0find` client.

the V^0 particle's momentum $\vec{p}_V$ and lying in the plane spanned by $\vec{p}_V$ and the y axis (fig. **??**) has to be in certain range.

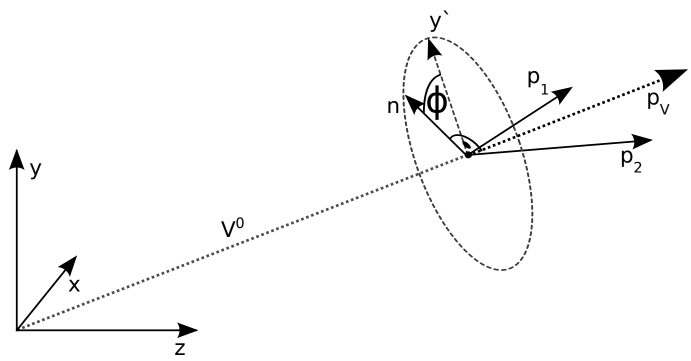

Figure 4.3: Graphical explanation of ϕ angle used by `v0find` client.

All conditions that tracks and V^0 candidate have to meet are summarized in the table 4.2.

4.2.2 v0fit

Found V^0 candidates are fitted by the `v0fit` client. It is done by a nine parameter Levenburgh-Marquardt procedure. Nine parameters are coordinates of the decay vertex and momenta components of daughters particles. Decay vertex point and V^0 momentum is added to the data and sent

Table 4.2: Summary of cuts used by `v0find` and their values.

cut	required value
number of points	≥ 10 (VTPC-1)
	≥ 20 (VTPC-2)
z_{V^0}	≥ -555 cm
DCA-x, DCA-y	≤ 1 cm
y1miny2	≥ 0.75 cm
xtv0, ytv0	≤ 25 cm
ϕ	≥ 0.2 rad
	≤ 2.9 rad

to DSPACK.

4.3 Monte Carlo simulation

Because of limited acceptance of the detectors, hardware simulations are needed to estimate the effect of limited acceptance of the NA61/SHINE detector and inefficiency of the reconstruction software. The simulation chain can be divided into the following steps:

- Generate events with VENUS event generator [25].
- Simulate the passage of generated particles (π, K, p, K^0_S, etc.) through the NA61/SHINE detectors using the GEANT simulation tool [26]. This software leads the particles through the matter, calculates the probabilities of different interactions, decays or secondary particle production. Transported particles leave hits inside TPCs. The ionization charge produced in the gas volume is not followed by GEANT, though.
- Simulate response of the pads to the hits left in TPCs by passing particles including the distortions of electric and magnetic fields. This is done by `MTSIM` client application.
- The whole dataset is processed through the same reconstruction chain, which is used to reconstruct the experimental data.

After all these steps there is a dataset of exactly the same structure as experimental one with additional information about generated particles.

4.4 Data analysis tools

4.4.1 ROOT

ROOT [27] is an open source, C++ based data processing and analysis framework maintained at CERN. Initially it was developed for NA49 and is now used worldwide by many experiments (including ALICE and STAR). It can be used on many different platforms an operating systems (e.g. Linux, Mac OS X, Microsoft Windows). Thanks to the built-in C interpreter (CINT) it is possible to write prototypes of the macros fast as it removes the time consuming compile/link cycle.

Powerful mathematical and statistical tools are provided within the framework. These tools, along with the power of a full featured C++ application and parallel processing allow for the most complex data manipulation.

ROOT provides full featured tools for data visualization. The data can be presented as histograms of various types, scatter plots, fitting functions and more. The graphical output can be easily adjusted using the tools provided. The high quality plots can be exported to different formats: eps, pdf, png and many others. This allows to include the results to the documents with minimal image manipulation.

The ROOT framework allows to save any object used in the script as a compressed binary `*.root` file. The data can be then sent over internet or accessed locally.

ROOT can be also used for building interactive, GUI-based applications.

4.4.2 ROOT61

ROOT61 [28] consists of two libraries, which add new functionality and data structures needed by the NA61/SHINE analysis to the ROOT framework. It is maintained by the NA61/SHINE collaboration. It evolved from the NA49 version, ROOT49.

ROOT61 libraries contain classes used for storing and accessing DST data ("T49DST") as well as full set of tools used in its analysis ("T49ANA"). Using the libraries, it is possible to apply event and track cuts, perform event mixing, $\frac{\mathrm{dE}}{\mathrm{dx}}$ analysis, and other NA61 specific operations. ROOT61 framework also include the DSPACK interface class, "TRootDS", for the conversion from DST format to its simplified version – mini-DST.
ROOT61 libraries can be downloaded from the official NA61 website.

Chapter 5

Analysis

The aim of the analysis was to produce the transverse momentum and rapidity distributions of neutral strange particles, namely K^0_S from a set of fitted V^0 candidates. To achieve the goal following steps have to be taken:

- datasets selection/generation,
- event selection,
- applying cuts on V^0 candidates to reduce background,
- signal extraction to produce raw spectra,
- calculating corrections for efficiency and acceptance.

5.1 Dataset selection

Both, experimental and Monte Carlo data, were collected/generated in 2007 and reconstructed using the standard NA61/SHINE reconstruction chain (version v1r4-1). Experimental dataset contains 454411 events of 30.9A GeV proton beam interacting with 2 cm thick, 1.84 g/cm^3 isotropic graphite target, used for T2K analysis. Monte Carlo dataset consists of 993127 events of the same interaction type, generated using VENUS event generator.

5.2 Events selection

Not all events from selected datasets represent proper interactions. Some of them could not have been reconstructed correctly because of beam instability or reconstruction software's malfunction. There is also a number of events in which beam protons did not interact within the target, but, for example, with one of detectors' shields instead. All those events have to be cut out to provide as reliable dataset as possible.

5.2.1 BPD vertex cut

It is important to make sure, that the interacting particles came with the beam. This is achieved by applying cut on BPDs' signals (fig. 5.1). Only events that have BPD vertex fitted using BPD-3 x and BPD-3 y are used in further analysis.

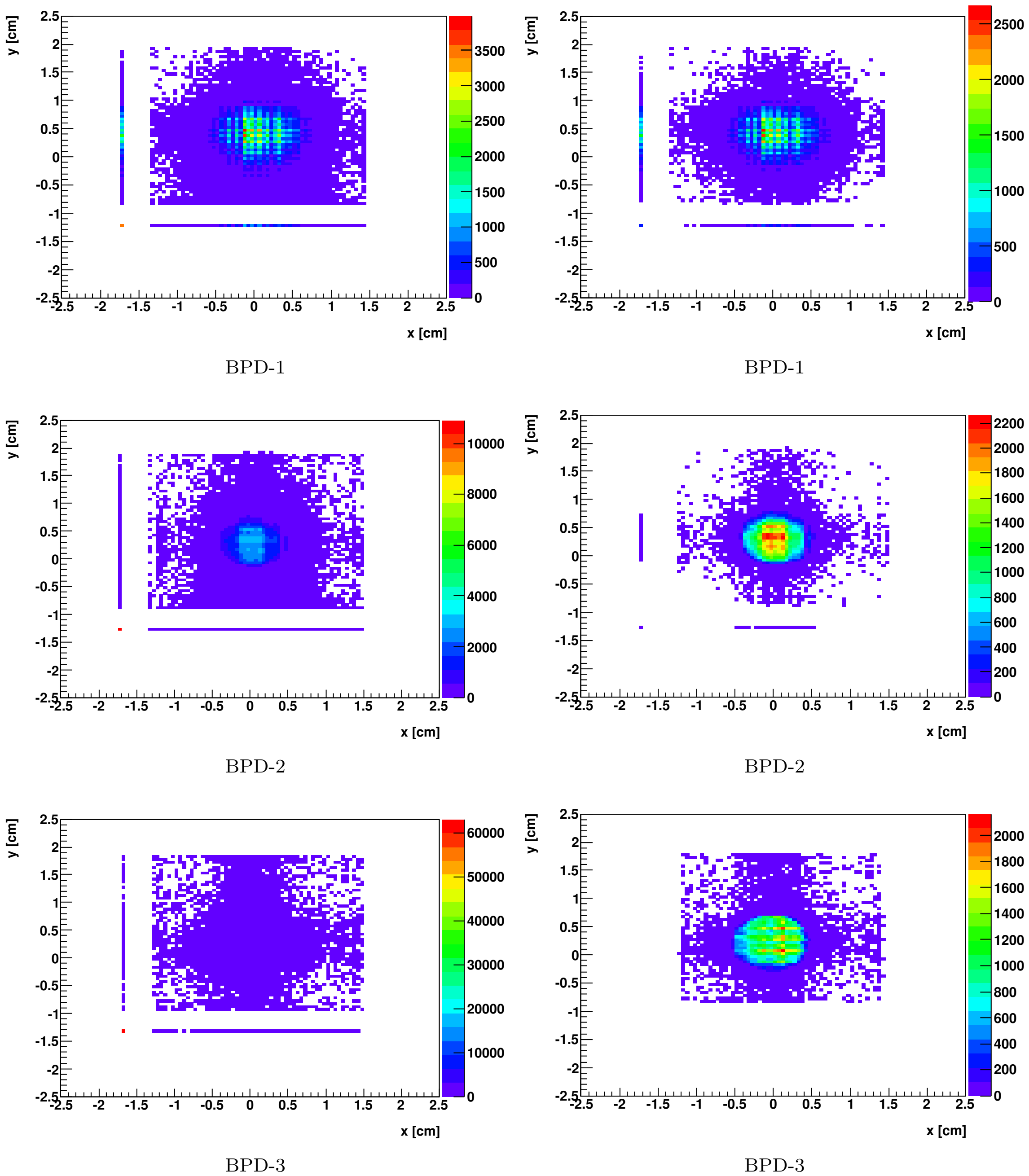

Figure 5.1: BPD profiles before (left) and after (right) the BPD vertex cut.

After applying this cut, there are 39% experimental data events less, but all those that left have a good quality BPD vertex. The cut was not applied to MC data as it does not contain beam information.

5.2.2 Fitted vertex existence cut

For some reasons, in some cases the reconstruction software might not be able to determine the fitted vertex (interaction point). Such events have to be cut out as they might not be beam particles' interactions but for example some cosmic-ray particles.

After applying the cut there are 12% experimental and 5% MC data less, but all those that left have fitted vertex.

5.2.3 Fitted vertex quality cut

Another issue that has to be taken into account is the fitted vertex quality. It may happen that even if the vertex has been successfully determined, there were some problems with the reconstruction. Those events also have to be cut out.

After applying the cut there are 13% experimental and 6% MC data less, but all those that left have a good quality fitted vertex.

5.2.4 Fitted vertex z coordinate cut

It is also important to select events, in which interaction took place within the target. Only events with fitted vertex z coordinate between -575 and -585 cm are taken for further analysis (fig. 5.2).

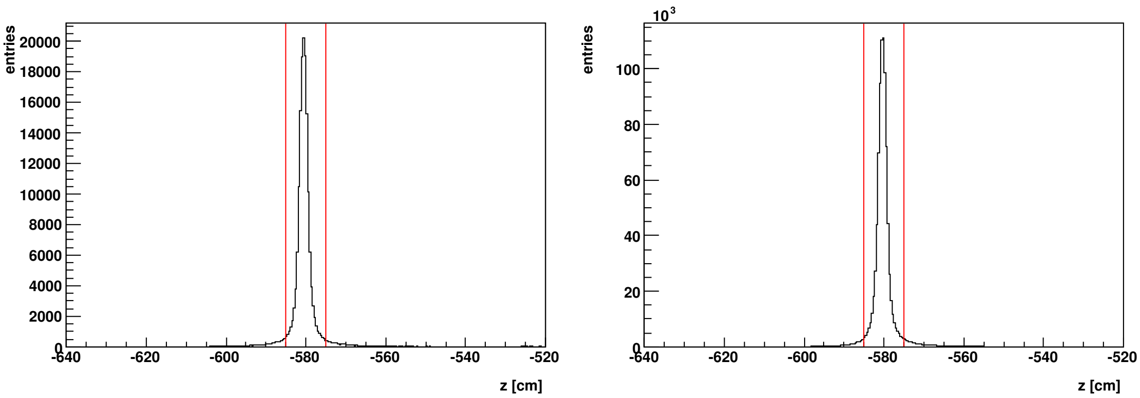

Figure 5.2: Fitted vartex z coordinate values in experimental (left) and Monte Carlo (right) data with cut values marked as red vertical lines.

After applying the cut, there are 5% experimental and 7% MC data less, but all those that left have interacted within the target.

5.2.5 Event cuts summary

Summary of event cuts' effect on both, experimental and MC data, is shown in table 5.1. After all cuts only 1/3 experimental data left, but all of them for sure represent interactions within the target with a good quality fitted vertex.

Table 5.1: Summary of event cuts' effects.

	Experimental data		Monte Carlo data	
	N_{events}	% of all	N_{events}	% of all
Before cuts	454411	100	993127	100
BPD vertex	176753	38.90	-	-
Fitted vertex existence	51254	11.28	49831	5.02
Fitted vertex quality	57737	12.71	58994	5.94
Fitted vertex z coord.	21209	4.67	66892	6.74
Events left	147458	32.45	817410	82.31

5.3 All V^0 candidates

After rejecting wrong events, 40818 V^0 candidates in experimental and 211332 in MC data were found. However some of them might be results of reconstruction software's malfunction. Also, not all of them are K^0_S particles. To learn more about those V^0s, kinematic properties of their decays are studied.

5.3.1 Invariant mass analysis

Reconstructed V^0 decay could be one of following: $K^0_S \rightarrow \pi^+ + \pi^-$, $\Lambda \rightarrow p + \pi^-$ or $\bar{\Lambda} \rightarrow \bar{p} + \pi^+$. The invariant mass of the decaying particle can be calculated according to the equation:

$$m_{INV} = \frac{1}{c^2}\sqrt{\left(\sum_i E_i\right)^2 - \left|\sum_i \vec{p_i}\right|^2 c^2},$$

where p_i denote decay products' momentum vectors and E_i – their energies. K^0_S hypothesis is tested by assuming that both decay's products are pions. Hence in natural units ($c \equiv 1$), knowing, that $E_i = \sqrt{m_i^2 + p_i^2}$, the equation becomes the following:

$$m_{INV} = \sqrt{2\left(m_\pi^2 + E_{\pi^+}E_{\pi^-} - \vec{p}_{\pi^+}\vec{p}_{\pi^-}\right)}.$$

Invariant mass of all V^0 candidates under K^0_S hypothesis is shown in figure 5.3.

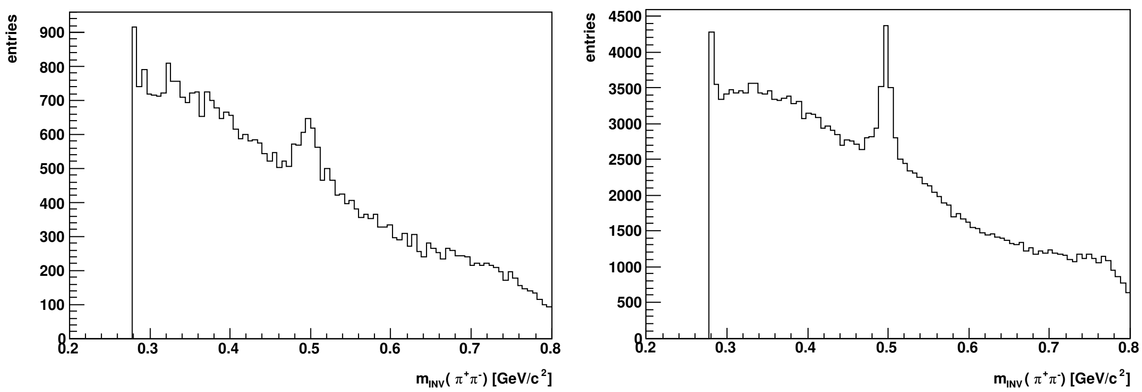

Figure 5.3: Invariant mass histograms of all V^0 candidates with K^0_S hypothesis in experimental (left) and Monte Carlo (right) data.

5.3.2 The Armenteros-Podolanski plot

The Armenteros-Podolanski plot [29] is another method of checking what type of V^0 particle was reconstructed. It is a two dimensional plot of Armenteros transverse momentum p_T^{Arm} and longitudinal momentum asymmetry α of oppositely charged decay products. First one is defined as the absolute value of one daughter particle's momentum component transverse to the original V^0 direction of motion (fig. 5.4):

$$p_T^{Arm} = p^{+,-} \sin \varphi^{+,-}.$$

The other variable, α, is defined as:

$$\alpha = \frac{p_L^+ - p_L^-}{p_L^+ + p_L^-}.$$

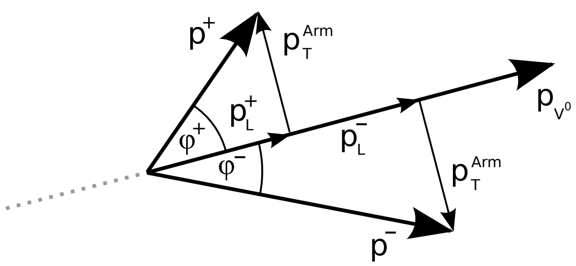

Figure 5.4: Explanation of p_T^{Arm}.

Possible decays of each V^0 draw half ellipses with centers lying on the α axis at a value defined by the daughter particle's mass difference. As K^0_S decays into two oppositely charged, but equally mass pions, center of its ellipse appears at $\alpha = 0$. Figure 5.5 illustrates how these half ellipses are situated in the plot.

The Armenteros-Podolanski plot of all V^0 candidates is shown in figure 5.6. There is a clear signal from K^0_S particles, but there are also a lot of Λs and some $\bar{\Lambda}$s.

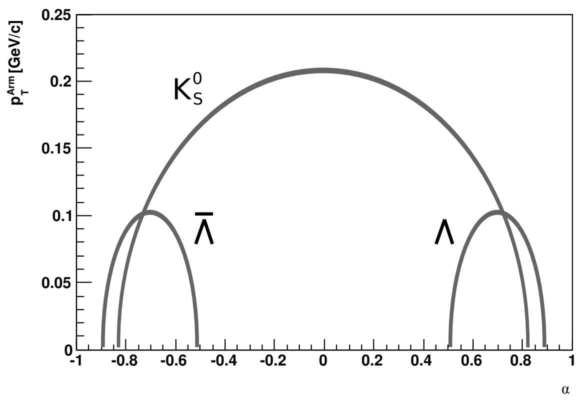

Figure 5.5: Theoretically allowed p_T^{Arm} and α values for strange neutral particles.

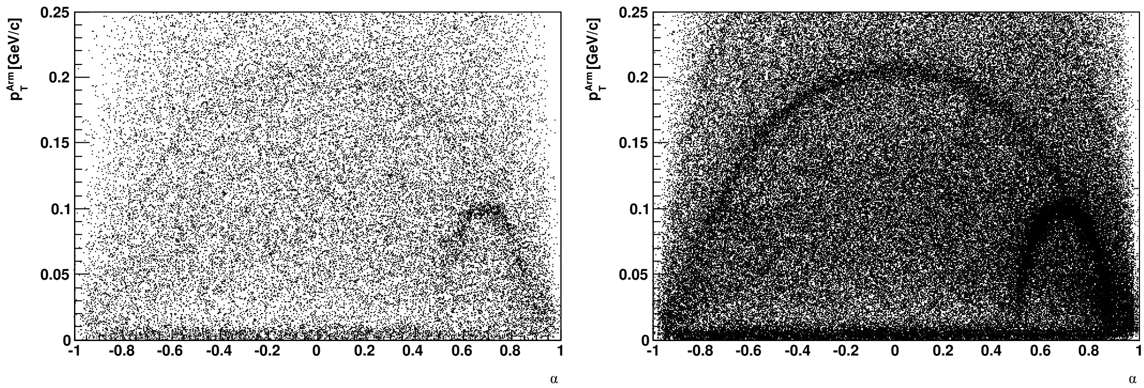

Figure 5.6: Armenteros-Podolanski plot for all V^0 candidates in experimental (left) and Monte Carlo (right) data.

5.4 V^0 selection

Although there is a clear K^0_S signal on the invariant mass histogram (fig. 5.3), the background is much too high. Series of V^0 cuts have to be applied to reduce it.

5.4.1 Invariant mass cut

As the K^0_S mass is known, a cut on invariant mass is introduced. All V^0s with invariant mass less then 0.35 or greater than 0.65 GeV/c^2 are cut out (fig. 5.7).

After applying the cut there are 40% less V^0s in both experimental and MC data.

5.4.2 Impact parameters cut

One of the tests performed by reconstruction chain's client (`v0find`) is checking the distance between the fitted vertex and V^0 candidate's x and y coordinates ("xtv0" and "ytv0") in fitted vertex plane. As a result, all found V^0s are for sure produced close to the main interaction ($\geq$ 25

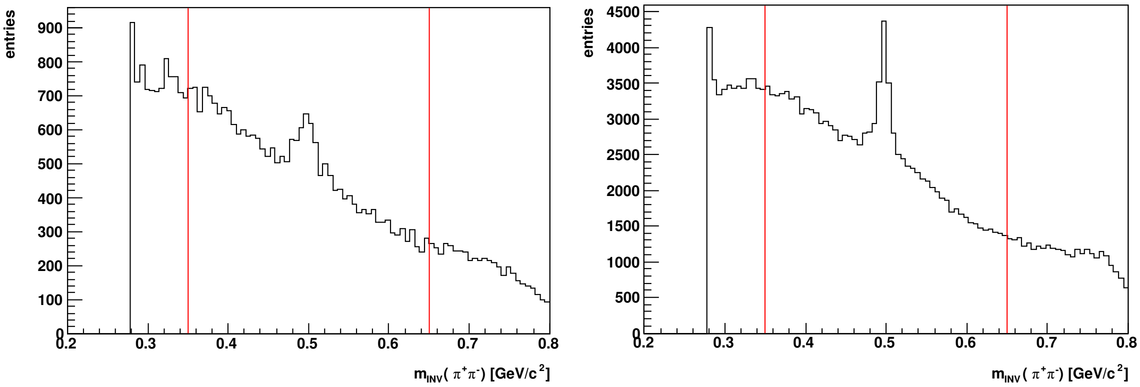

Figure 5.7: Same as figure 5.3 with invariant mass cut values marked as vertical red lines.

cm). The cut's values are too wide, though. Additional cut is applied. All V^0 candidates which are assumed to be produced further than 10 cm from the fitted vertex are not taken to further analysis.

Applying the cut rejects 1% V^0s from both experimental and MC data.

5.4.3 cos θ^* cut

Another cut applied to V^0s is the cut on $\cos\theta^*$. It is an angle between K^0_S candidate and its decay products' momenta in the center of mass coordinate system (fig. 5.8).

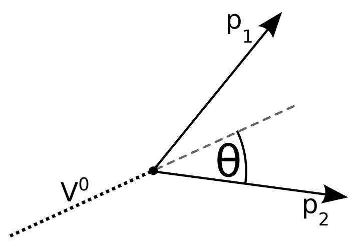

Figure 5.8: Explanation of $\cos\theta^*$

As K^0_S is a spinless particle, its decay products' distribution must be isotropic in its rest frame. Therefore $\cos\theta^*$ distribution is expected to be flat. However, because of wrongly matched tracks during the reconstruction, there are too many particles with $\cos\theta^*$ close to -1 and 1 (fig. 5.9). This cut is applied to reject those V^0s, which daughters' $\cos\theta^*$ value is not within flat region on the histogram, i.e. $-0.95 < \cos\theta^* < 0.8$ (fig. 5.9).

This cut rejects 18% V^0 candidates in experimental and 20% in MC data.

5.4.4 Δz cut

As primary tracks naturally come together at the fitted vertex, they can be mistakenly considered as V^0 daughters' tracks by the reconstruction software. A cut on V^0 candidates' decay vertex

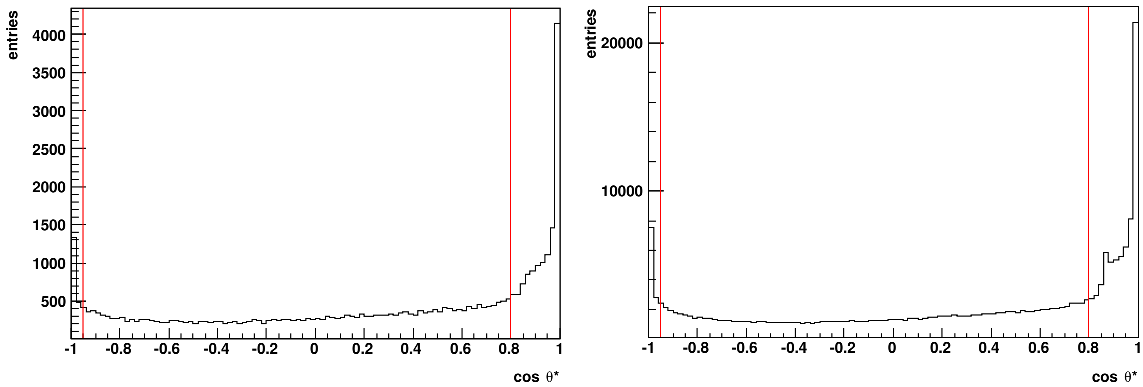

Figure 5.9: $\cos\theta^*$ histograms of all V^0 candidates in experimental (left) and Monte Carlo (right) data with $\cos\theta^*$ cut values marked as vertical red lines.

z coordinate have to be applied. It insists that the difference (Δz) between fitted vertex's and V^0 candidate's z is in certain range. Δz values of all V^0 candidates are shown in figure 5.10.

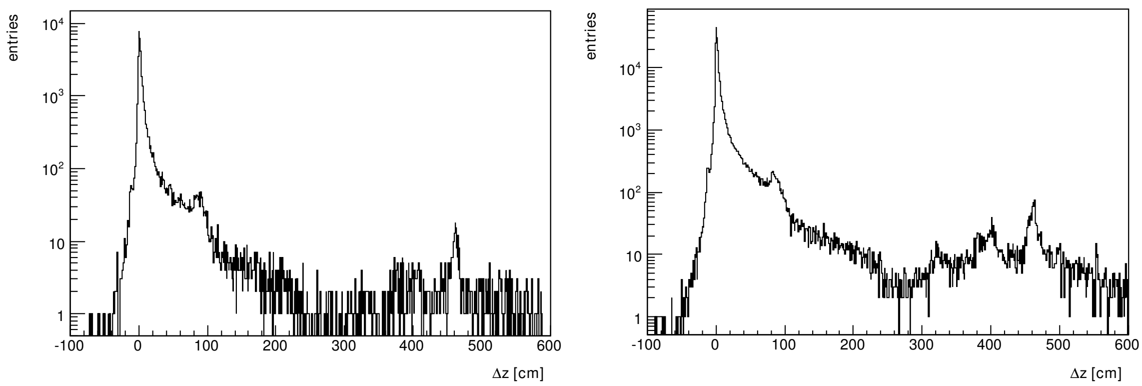

Figure 5.10: Δz histograms of all V^0 candidates in experimental (left) and Monte Carlo (right) data.

In order to find optimal values of minimum and maximum Δz, Significance S was introduced. It describes a "signal-to-background" ratio and is defined as:

$$S = \frac{\int\limits_{x_0-\frac{3}{2}\Gamma}^{x_0+\frac{3}{2}\Gamma} Signal(x)\,\mathrm{d}x}{\sqrt{\int\limits_{x_0-\frac{3}{2}\Gamma}^{x_0+\frac{3}{2}\Gamma} Signal(x)\,\mathrm{d}x + \int\limits_{x_0-\frac{3}{2}\Gamma}^{x_0+\frac{3}{2}\Gamma} Background(x)\,\mathrm{d}x}}$$

where *Signal* and *Background* are invariant mass histogram's fit functions, x_0 and Γ are their parameters. The signal peak is fitted with a lorentzian function:

$$Signal(x) = A\frac{1}{\pi}\frac{\frac{1}{2}\Gamma}{(x-x_0)^2 + \left(\frac{1}{2}\Gamma\right)^2}$$

where A is a parameter introduced to control peak's height, Γ is its full width at half maximum (FWHM) and x_0 is its mean value (i.e. K^0_S expected mass). Histogram's background is fitted with a 4$^{\text{th}}$ order polynomial function:

$$Background(x) = a_0 + a_1 x + a_2 x^2 + a_3 x^3 + a_4 x^4$$

where a_0, a_1, a_2, a_3 and a_4 are the polynomial's coefficients. To find minimum and maximum cuts' values, significance was calculated for different Δz. For each step invariant mass histogram had to be plotted and fitted as illustrated in figure 5.11.

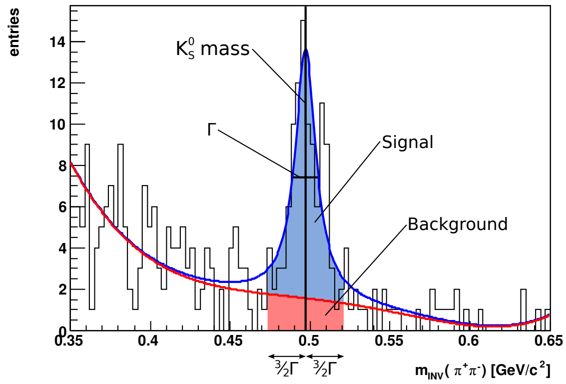

Figure 5.11: Illustration of the invariant mass histogram fitted with *Signal* and *Background* functions used for Significance calculation.

Obtained values of significance are shown in figure 5.12.

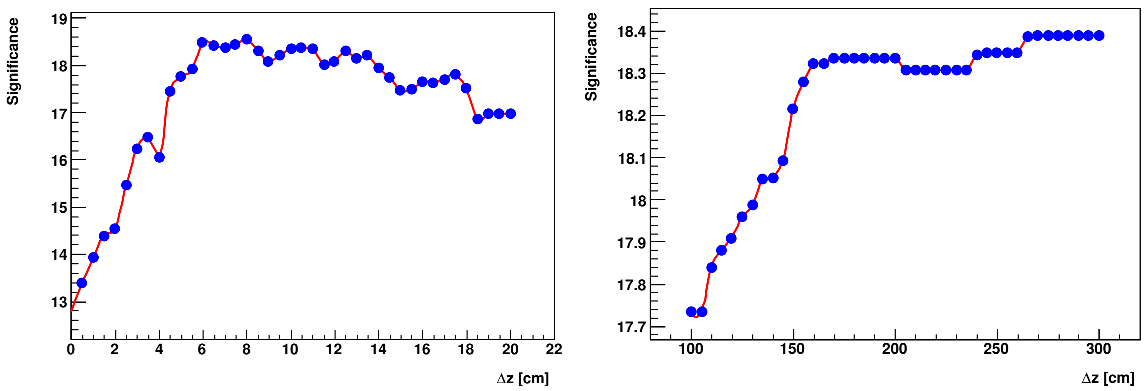

Figure 5.12: Minimum (left) and maximum (right) Significance graphs for experimental data.

Taking maximum significance values for given ranges and having in mind that every cut reduces the statistics, Δz cut is set to $6 < \Delta z < 270$ cm. The same values are applied to MC data. The cut is shown in figure 5.13.

This cut rejects 37% of experimental and 35% of MC data V^0 candidates.

5.4.5 V^0 cuts summary

Summary of V^0 cuts' effect on both experimental and MC data is shown in table 5.2. After all cuts, only 5% K^0_S candidates left in experimental data.

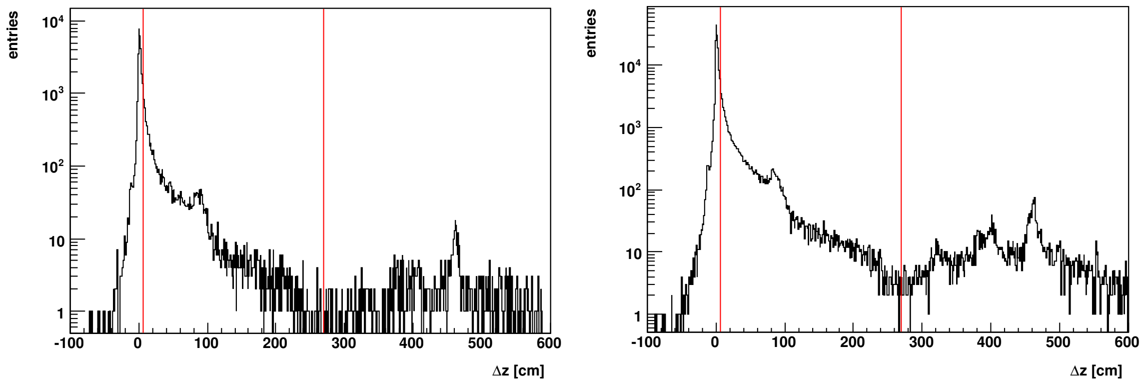

Figure 5.13: Same as figure 5.10 with cut values marked as red vertical lines.

Table 5.2: Summary of V^0 cuts' effects.

	Experimental data		Monte Carlo data	
	N_{V^0}	% of all	N_{V^0}	% of all
Before cuts	40818	100	211332	100
Invariant mass	16258	39.83	85304	40.36
Impact parameters	474	1.16	1324	0.63
$\cos\theta^*$	7101	17.40	41204	19.50
Δz	14884	36.46	73336	34.70
V^0s left	2101	5.15	10164	4.81

Invariant mass histogram of V^0s that passed all cuts is shown in figure 5.14. Significant background reduction in comparison to figure 5.3 can be observed.

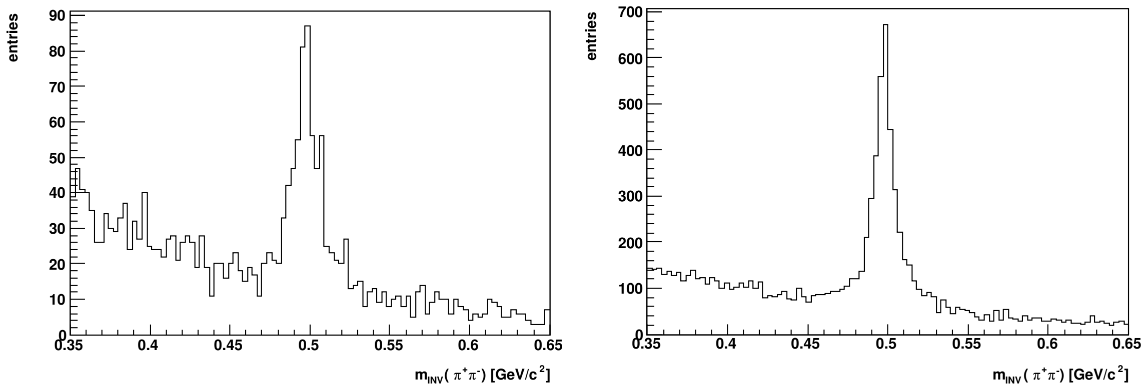

Figure 5.14: Invariant mass histograms of selected V^0 candidates with K^0_S hypothesis in experimental (left) and Monte Carlo (right) data.

Armentheros-Podolanski plots of both experimental and Monte Carlo data after cuts are shown in figure 5.15. Significant non-K^0_S background reduction in comparison to figure 5.6 is observed.

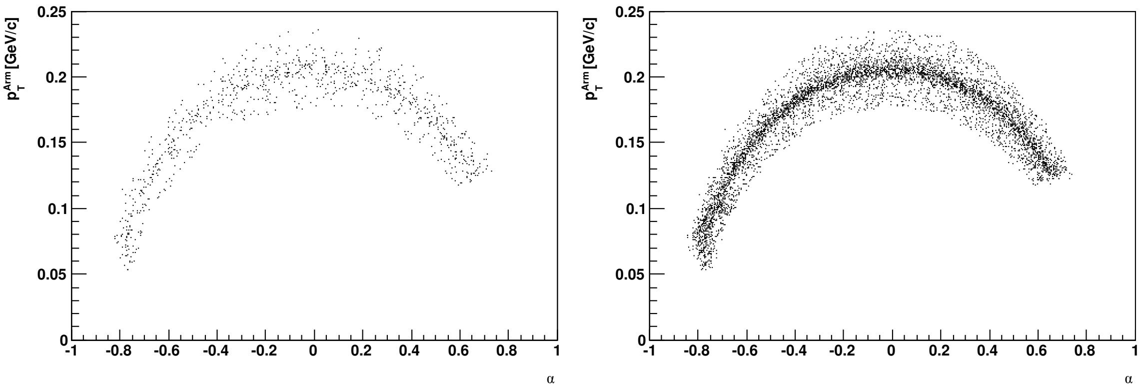

Figure 5.15: Armenteros-Podolanski plot of selected V^0 candidates in experimental (left) and Monte Carlo (right) data.

5.5 Binning

It is not the total K^0_S particles' production, but its distribution in rapidity and transverse momentum in the interest of the analysis. Data has to be divided into bins and all further analysis is done on bin-by-bin basis. Size of the bins is determined by the statistics. A compromise has to be reached, as the smaller bins are, the better results can be achieved, but dividing data into subsets significantly decreases statistics in bins. Monte Carlo data is binned in the same way as experimental data.

To learn about production of K^0_S particles with different transverse momenta, six bins of equal size from p_T = 0 to p_T = 1.2 GeV/c are introduced (fig. 5.16 left). Similarly, to produce spectra with respect to center-of-mass rapidity, data is divided into six bins from y* = -0.5 to y* = 1 (fig. 5.16 right).

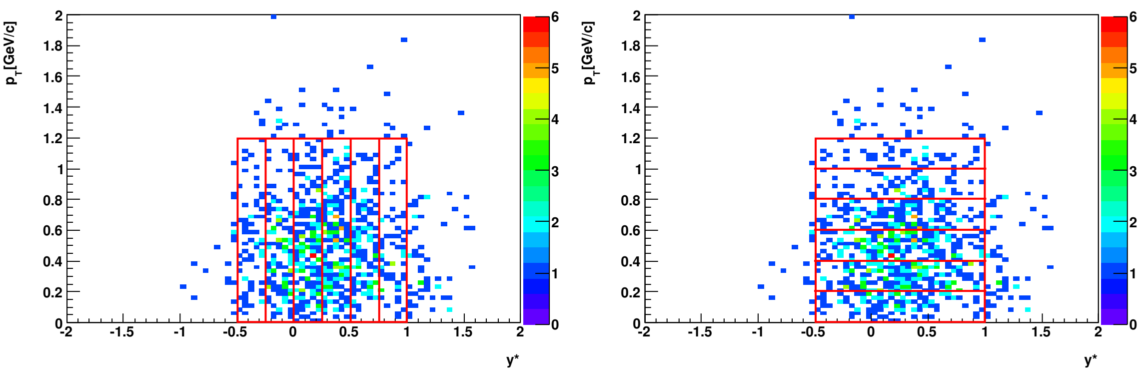

Figure 5.16: p_T-y* histograms with binning marked with red lines for different binning types

5.6 Uncorrected distributions

After most of the combinatorial background has been removed by V^0s' cuts, raw spectra can be evaluated. Invariant mass histogram is produced in each bin. Then it is fitted by *Signal* and *Background* functions (section 5.4.4). Figures 5.17 and **??** show fitted invariant mass histograms for all rapidity and transverse momentum bins respectively.

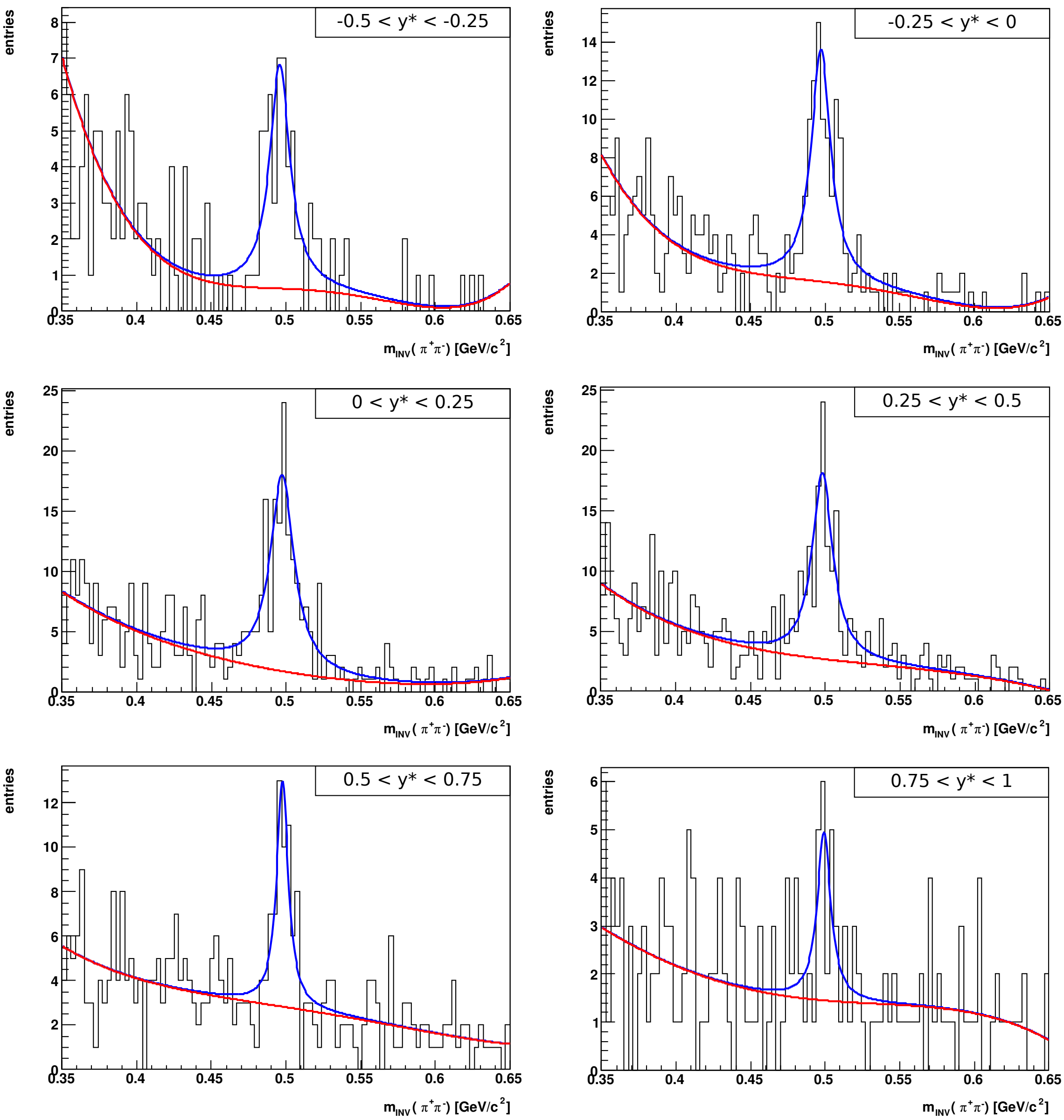

Figure 5.17: Invariant mass histograms in each rapidity bin fitted with *Signal* and *Backgroud* functions.

Number of K^0_S particles is evaluated as an integral from the signal function ±20 MeV around K^0_S mass as illustrated in figure 5.19.

Calculation results for both ways of binning are shown in figure 5.20.

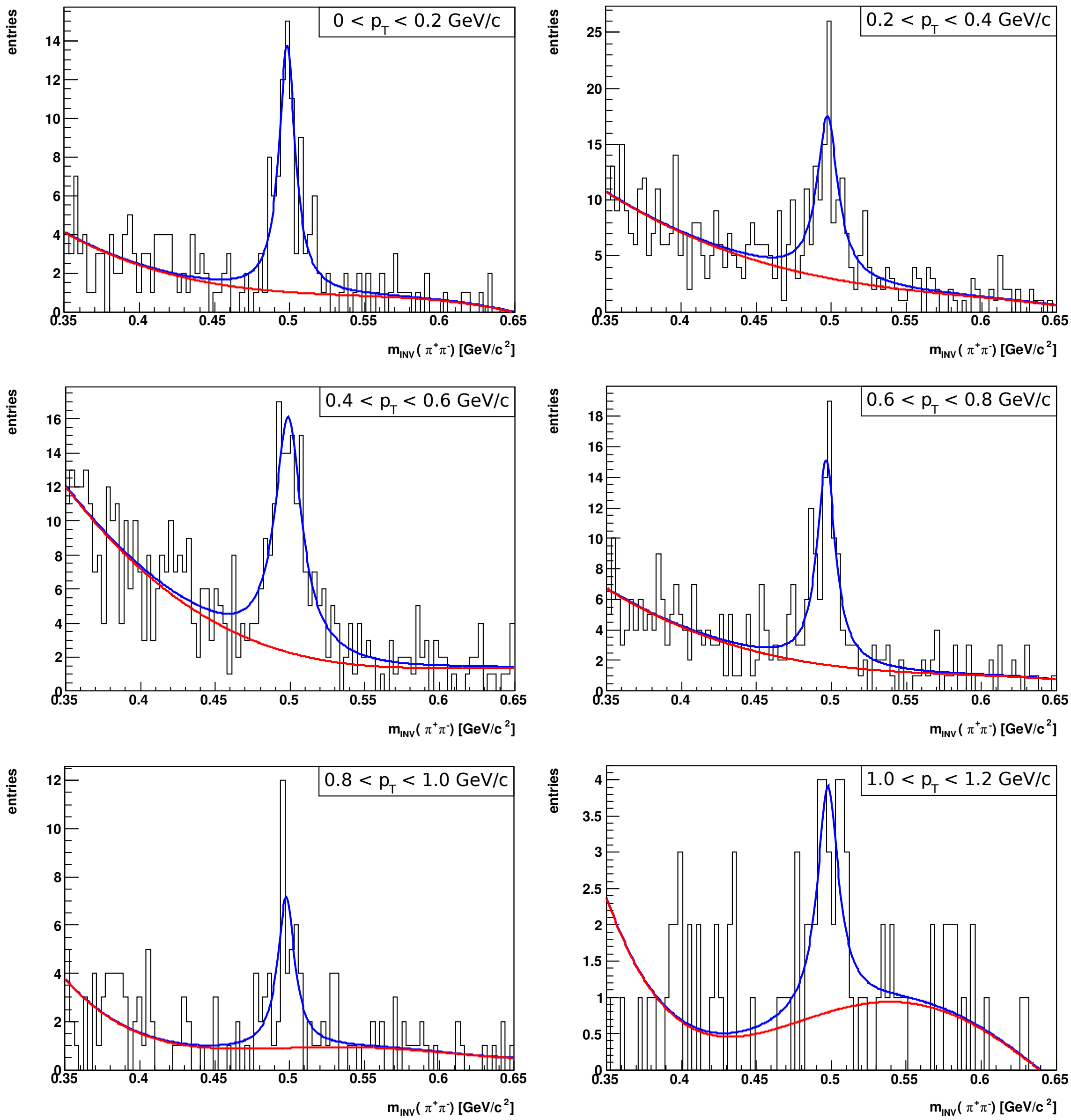

Figure 5.18: Invariant mass histograms in each transverse momentum bin fitted with *Signal* and *Backgroud* functions.

5.7 Efficiency and acceptance correction

Obtained raw distributions (fig. 5.20) show all K^0_S that have been reconstructed. But, for various reasons, not all particles could be found. To show all those produced in the p+C at 30.9A GeV collision, correction need to be applied.

One of the corrections is the acceptance correction, which takes into account the geometrical acceptance of the detector. The other is the efficiency correction, that corrects data for both reconstruction software's and detector's inefficiencies. Figure 5.21 illustrates p_T-y^* distributions of all K^0_S particles generated by VENUS event generator (top left), selected V^0s in MC data (top right) and selected V^0s in experimental data (bottom). Effect of limited detector acceptance and

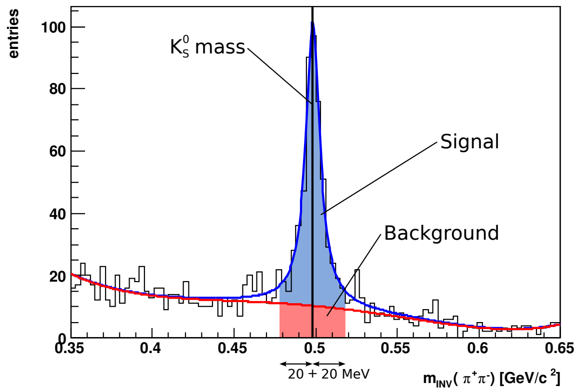

Figure 5.19: Illustration of the invariant mass histogram in one of the bins fitted with *Signal* and *Background* functions used for calculation of the number of K^0_S particles in that bin.

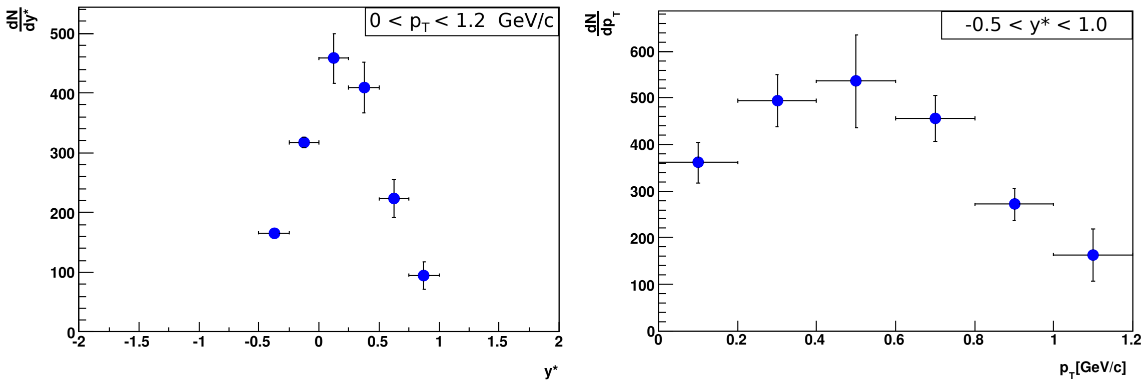

Figure 5.20: Uncorrected distributions of K^0_S

software inefficiencies can be observed.

Efficiency correction is calculated by comparing number of K^0_S in Monte Carlo data generated for the analysis with K^0_S number in the same data after reconstruction (fig. 5.22) using the formula:

$$\epsilon = \frac{N_{K^0_S\ accepted}}{N_{K^0_S\ generated}}.$$

Its error was evaluated using binomial distribution:

$$\Delta\epsilon = \sqrt{\frac{N_{K^0_S\ accepted} \times N_{K^0_S\ rejected}}{N^3_{K^0_S\ generated}}} = \sqrt{\frac{\epsilon\,(1-\epsilon)}{N_{K^0_S\ generated}}}.$$

Correction factors for both binning ways are presented in figure 5.23.

5.8 Corrected distributions

Figure 5.24 illustrates K^0_S distributions after applying efficiency and acceptance correction.

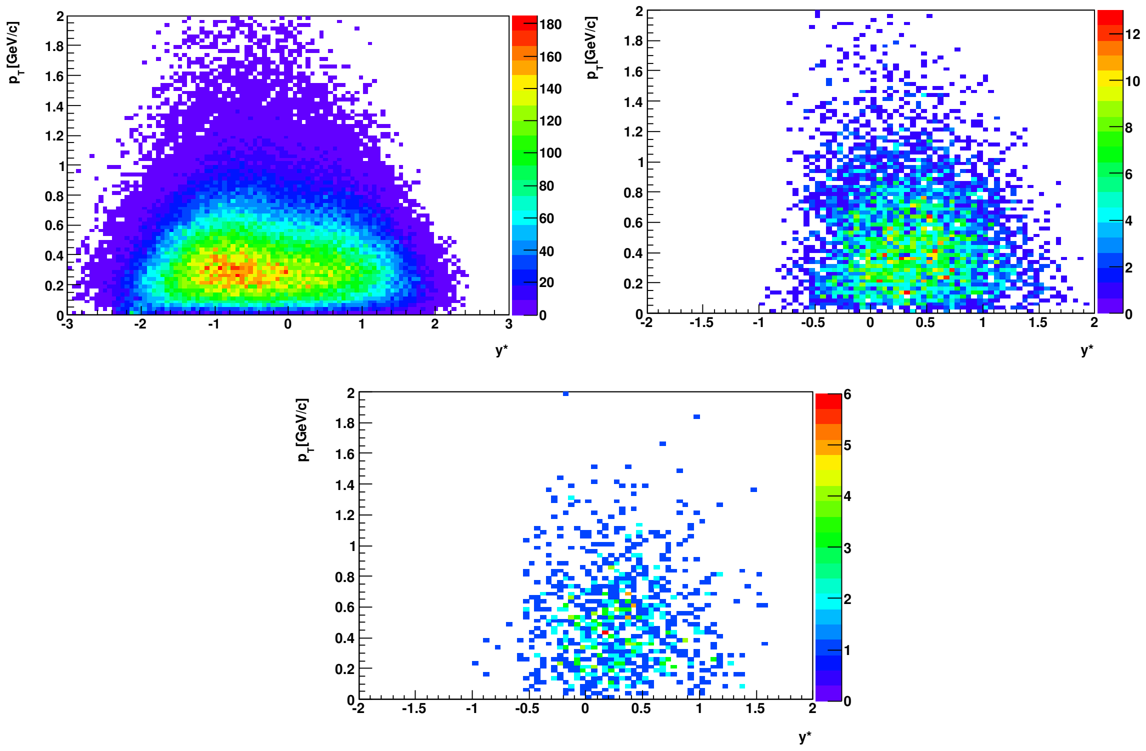

Figure 5.21: p_T-y^* distributions of all K^0_S particles generated by VENUS event generator (top left), selected V^0s in MC data (top right) and selected V^0s in experimental data (bottom).

5.9 Correction for inelastic events cut out

Due to event cuts that are applied some inelastic events might be cut out. To correct the data for their rejection Monte Carlo simulations are used. VENUS event generator generates only inelastic interactions. Factor of cut out inelastic events is calculated as:

$$\epsilon_{events} = \frac{N_{events\ MC\ accepted}}{N_{events\ MC\ generated}} = \frac{817410}{993127} = 0.823$$

and is applied to experimental data to obtain corrected inelastic number of events:

$$N_{inel} = \frac{N_{events\ accepted}}{\epsilon_{events}} = \frac{147458}{0.823} = 179156.$$

That gives total number of events representing inelastic interactions $N_{inel} = 179156$.

5.10 Normalization

Both experimental and Monte Carlo data should be normalized to the number of inelastic events. That allows to compare them with each other. Monte Carlo data is normalized to the number of all events generated by VENUS as all of them are inelastic interactions. Experimental data is normalized to corrected number of inelastic events, N_{inel}.

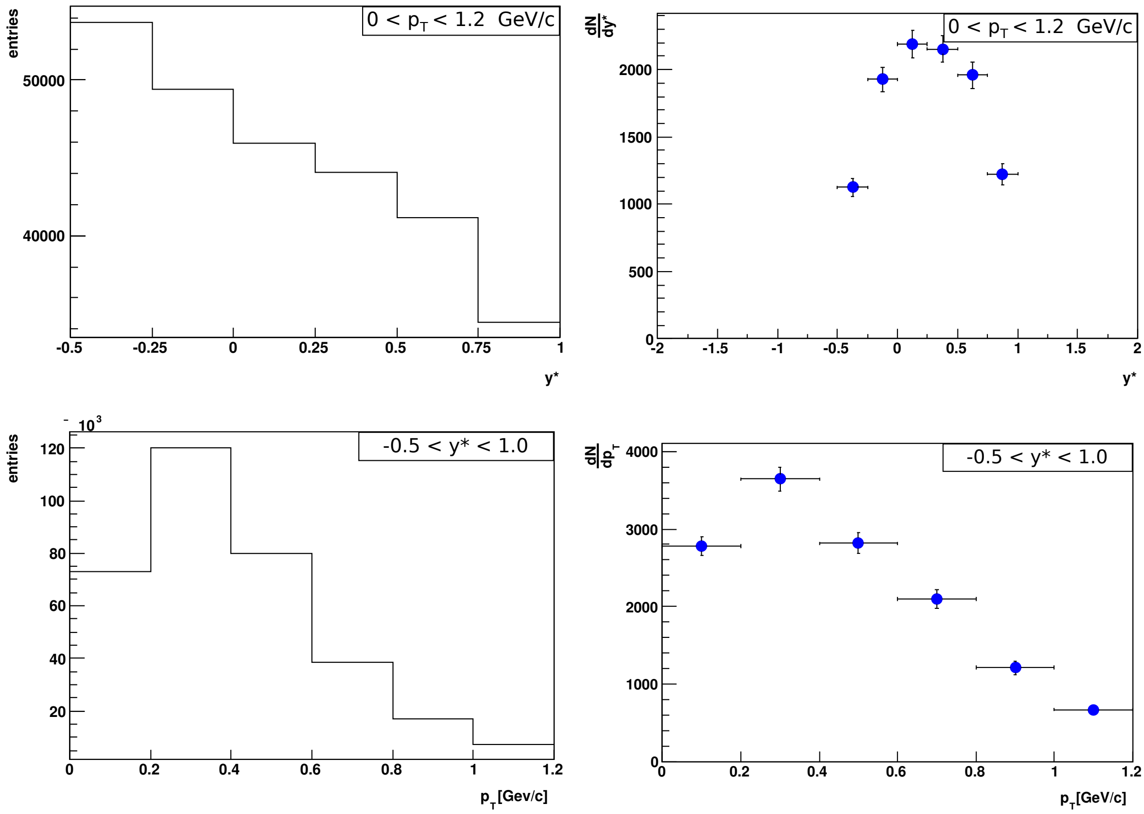

Figure 5.22: K_S^0 particles generated (left) and found after the standard NA61/SHINE reconstruction procedure (right) for different binning ways.

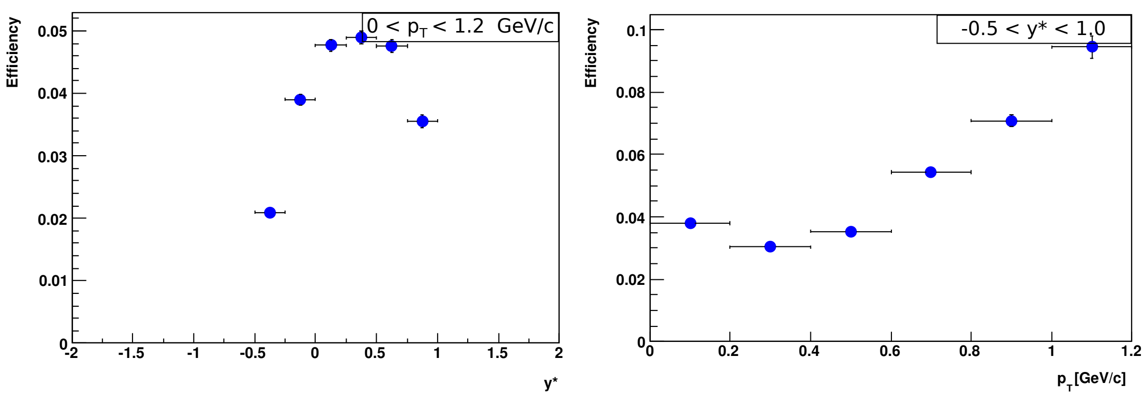

Figure 5.23: Correction factors for both binning ways

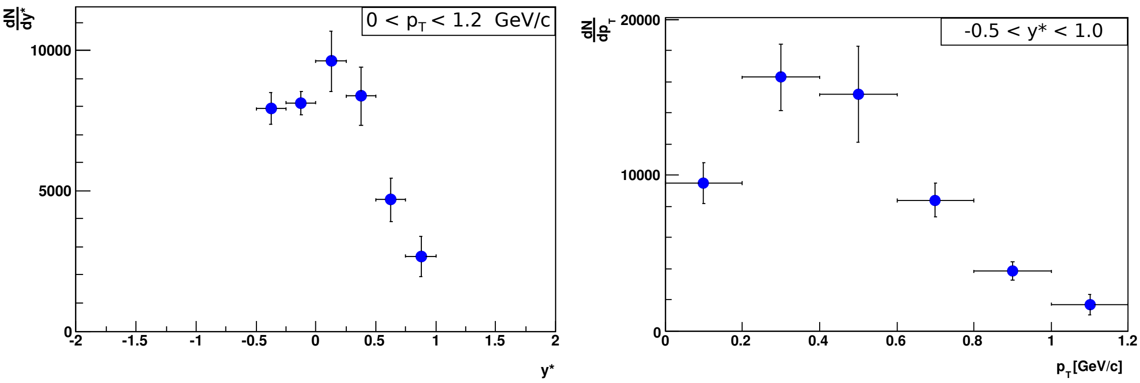

Figure 5.24: Corrected distributions of K^0_S

Chapter 6

Results and discussion

6.1 Final K^0_S distributions

Final K^0_S distributions are normalized to the number of inelastic interactions as discussed in section 5.10.

6.1.1 p_T and m_T distributions

Final p_T distribution of K^0_S (integrated over rapidity values from -0.5 to 1) are shown in figure 6.1. In addition to the plot, results of analysis are listed in table 6.1.

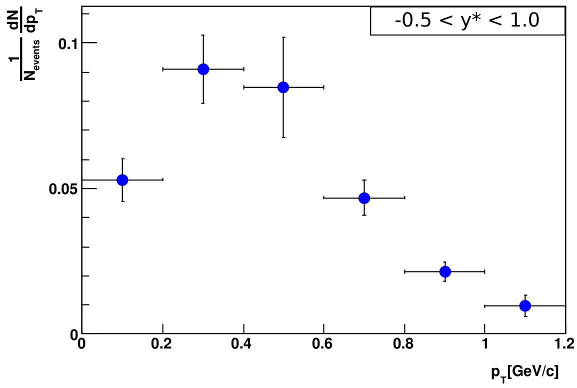

Figure 6.1: K^0_S final p_T distribution.

For low transverse momentum values the distribution can be described by the formula:

$$\frac{dN}{dp_T} \propto p_T exp\left[-\frac{m_T}{T}\right],$$

where T denotes inverse slope parameter and m_T – transverse mass: $m_T = \sqrt{m^2 + p_T^2}$. The inverse slope parameter can be interpreted as the effective temperature of the system at the freeze-out plus additional art connected with radial motion. Transverse mass distribution follows the formula:

$$\frac{dN}{dm_T} \propto m_T exp\left[-\frac{m_T}{T}\right],$$

Table 6.1: Results of p_T distribution analysis.

p_T [GeV/c]	Uncorrected K^0_S	Efficiency correction	Corrected, normalized K^0_S
0 – 0.2	361 ± 43	0.03799 ± 0.00071	0.05305 ± 0.00731
0.2 – 0.4	494 ± 56	0.03032 ± 0.00049	0.09094 ± 0.01179
0.4 – 0.6	536 ± 99	0.03529 ± 0.00065	0.08479 ± 0.01723
0.6 – 0.8	456 ± 49	0.05433 ± 0.00115	0.04685 ± 0.00603
0.8 – 1	272 ± 35	0.07082 ± 0.00196	0.02144 ± 0.00335
1 – 1.2	163 ± 56	0.09448 ± 0.00348	0.00963 ± 0.00366

hence m_T distribution can be obtained from p_T distribution:

$$\frac{1}{m_T}\frac{dN}{dm_T} = \frac{1}{p_T}\frac{dN}{dp_T}.$$

Both transverse distributions were fitted with an exponential function of transverse mass and inverse slope parameter. Results are shown in figure 6.2. The red line marks the fit.

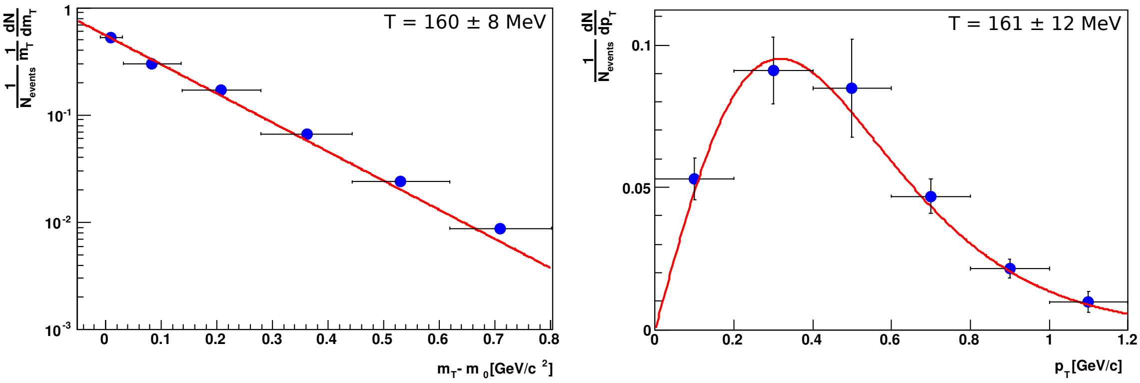

Figure 6.2: K^0_S m_T (left) and p_T (right) distributions fitted with exponential function.

6.1.2 y* distribution

Final rapidity distribution of K^0_S (with $p_T < 1.2$) are shown in figure 6.3. In addition to the plot, results of analysis are listed in table 6.2.

6.2 Distributions' shapes

Obtained distributions are compared with distributions of K^0_S particles generated by VENUS and normalized to the number of generated events. Experimental data is marked by blue points. Red lined histogram represents generated K^0_S. On both distributions in figure 6.4 fairy good agreement can be observed.

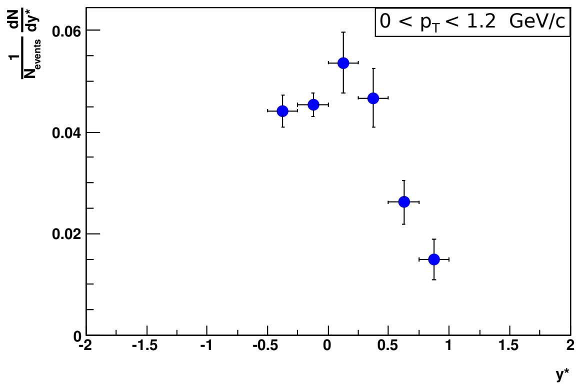

Figure 6.3: K^0_S final y* distribution.

Table 6.2: Results of y* distribution analysis.

y*	Uncorrected K^0_S	Efficiency correction	Corrected, normalized K^0_S
-0.5 – -0.25	166 ± 7	0.02096 ± 0.00062	0.04420 ± 0.00317
-0.25 – 0	317 ± 9	0.03900 ± 0.00087	0.04537 ± 0.00230
0 – 0.25	458 ± 42	0.04767 ± 0.00099	0.05363 ± 0.00604
0.25 – 0.5	409 ± 42	0.04889 ± 0.00103	0.04670 ± 0.00578
0.5 – 0.75	223 ± 32	0.04758 ± 0.00105	0.02616 ± 0.00433
0.75 – 1	95 ± 23	0.03558 ± 0.00100	0.01490 ± 0.00403

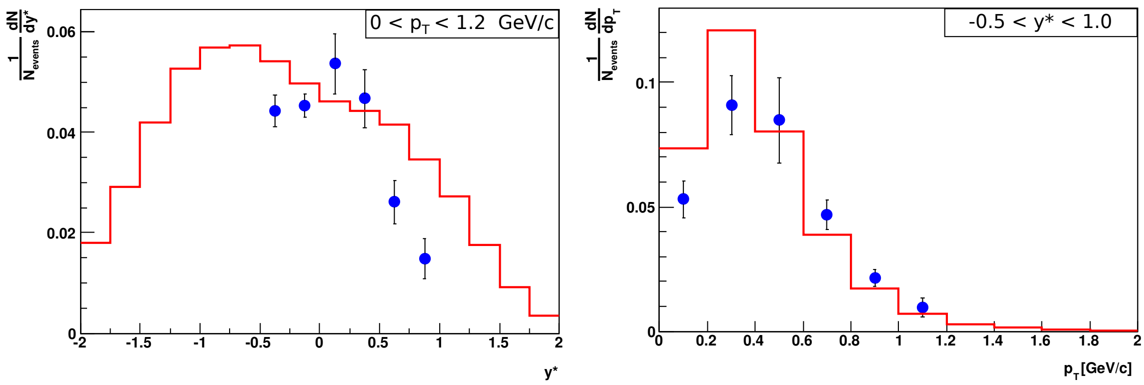

Figure 6.4: Comparison of K^0_S particles' y* (left) and p_T (right) distributions generated by VENUS (red line) and produced in NA61/SHINE (blue points).

Summary and conclusions

In this thesis production of K^0_S particles in the NA61/SHINE experiment was studied. Total number of over 454 thousand events representing proton-carbon interaction at the beam energy of 30.9A GeV ($\sqrt{s_{NN}} = 4.41$ GeV) collected in 2007 have been analyzed.

First, in both experimental and Monte Carlo data, cuts were applied to reject events, that didn't contain reliable information about the interaction. Then steps were taken to reduce background of invariant mass histograms. Next, data was divided into bins and fitted. After subtracting background, raw spectra of K^0_S were produced. Efficiency and acceptance corrections were calculated and applied to obtain final distributions. Finally, distributions were normalized to the number of inelastic events.

Unfortunately, because of poor statistics it was difficult to perform the analysis. Therefore data could be divided into only six bins in both rapidity and transverse momentum. Not only number of bins, but also their width and range of y^* and p_T leave room for improvement. As more points of the distributions could be obtained, more detailed study would be possible.

Also comparison with other experiments could extend discussion of the results of the analysis. Over the years, substantial amount of data on K^0_S (and strangeness in general) production were collected. That would allow to check if results are consistent with other experiments.

It would also be interesting to perform analysis for different beam energies to study the energy dependence of K^0_S production. In the future NA61/SHINE is planning to perform such analysis.

List of Figures

1.1 Elementary particles of the Standard Model. 4

1.2 Theoretical phase diagram of strongly interacting matter. 5

1.3 Time Projection Chamber scheme. 8

1.4 $\frac{\mathrm{dE}}{\mathrm{dx}}$ vs ToF for 1–2 GeV/c particles (NA61/SHINE). 9

3.1 Theoretical phase diagram region explored by NA61/SHINE and NA49. 14

3.2 The layout of NA61/SHINE experimental set-up top view (not to scale). 14

3.3 NA61/SHINE new DCS schema. 19

4.1 Samples of reconstructed events 21

4.2 Graphical explanation of cuts used by `v0find` client. 23

4.3 Graphical explanation of ϕ angle used by `v0find` client. 23

5.1 BPD profiles before and after the BPD vertex cut. 27

5.2 Fitted vartex z coordinate values in experimental and Monte Carlo data with cut values marked. 28

5.3 Invariant mass histograms of all V^0 candidates with K^0_S hypothesis in experimental and Monte Carlo data. 30

5.4 Explanation of p_T^{Arm}. 30

5.5 Theoretically allowed p_T^{Arm} and α values for strange neutral particles. 31

5.6 Armenteros-Podolanski plot for all V^0 candidates in experimental and Monte Carlo data. 31

5.7 Same as figure 5.3 with cut value marked. 32

5.8 Explanation of $\cos\theta^*$ 32

5.9 $\cos\theta^*$ histograms of all V^0 candidates in experimental and Monte Carlo data cut values marked. 33

5.10 Δz histograms of all V^0 candidates in experimental and Monte Carlo data. 33

5.11 Illustration of the invariant mass histogram fitted with *Signal* and *Background* functions used for Significance calculation. 34

5.12 Minimum and maximum Significance graphs for experimental data. 34

5.13 Same as figure 5.10 with cut values marked. 35

5.14 Invariant mass histograms of selected V^0s with K^0_S hypothesis in experimental and Monte Carlo data. 35
5.15 Armenteros-Podolanski plot of selected V^0s in experimental and Monte Carlo data. 36
5.16 p_T-y^* histograms with binning marked for different binning types 36
5.17 Invariant mass histograms in each rapidity bin fitted with *Signal* and *Backgroud* functions. 37
5.18 Invariant mass histograms in each transverse momentum bin fitted with *Signal* and *Backgroud* functions. 38
5.19 Illustration of the invariant mass histogram in one of the bins fitted with *Signal* and *Background* functions used for calculation of the number of K^0_S particles in that bin. 39
5.20 Uncorrected distributions of K^0_S 39
5.21 p_T-y^* distributions of all K^0_S particles generated by VENUS event generator, selected V^0s in MC data and selected V^0s in experimental data. 40
5.22 K^0_S particles generated and found after standard the NA61/SHINE reconstruction procedure for both binning ways. 41
5.23 Correction factors for both binning ways 41
5.24 Corrected distributions of K^0_S 42

6.1 K^0_S final p_T distribution. 43
6.2 K^0_S m_T and p_T distributions fitted with exponential function. 44
6.3 K^0_S final y^* distribution. 45
6.4 Comparisons of K^0_S particles' distributions generated by VENUS and produced in NA61/SHINE. 45

List of Tables

1.1 Summary of fundamental forces of the Standard Model. 5

2.1 K^0_S decay modes [13]. 12

3.1 Dimensions of NA61/SHINE TPC detectors. 15

4.1 Event reconstruction chain procedure. 22
4.2 Summary of cuts used by `v0find` and their values. 24

5.1 Summary of event cuts' effects. 29
5.2 Summary of V^0 cuts' effects. 35

6.1 Results of p_T distribution analysis. 44
6.2 Results of y^* distribution analysis. 45

Bibliography

[1] J. C. Collins and M. J. Perry, "Superdense Matter: Neutrons or Asymptotically Free Quarks?", Phys. Rev. Lett. **34**, 1353–1356 (1975)

[2] E. L. Bratkovskaya *et al.*, "Review of QGP signatures: Ideas versus observables", arXiv:nucl-th/0401031.

[3] T. Matsui and H. Satz, "J/Psi Suppression By Quark-Gluon Plasma Formation", Phys. Lett. B **178**, 416 (1986).

[4] D. G. d'Enterria, "Jet quenching: RHIC results and phenomenology", AIP Conf. Proc. **806** (2006) 252 [arXiv:nucl-ex/0510062].

[5] J. Rafelski and B. Muller, "Strangeness Production In The Quark-Gluon Plasma", Phys. Rev. Lett. **48**, 1066 (1982) [Erratum-ibid. **56**, 2334 (1986)].

[6] M. Rybczynski *et al.* [The NA49 Collaboration], "Multiplicity fluctuations in nuclear collisions at 158-A-GeV", J. Phys. Conf. Ser. **5**, 74 (2005) [arXiv:nucl-ex/0409009].

[7] C. Roland *et al.* [The NA49 Collaboration], "Event-by-event fluctuations of particle ratios in central Pb + Pb collisions at 20-A-GeV to 158-A-GeV", J. Phys. G **30**, S1381 (2004) [arXiv:nucl-ex/0403035].

[8] M. Gazdzicki *et al.* [NA49 Collaboration], "Report from NA49", J. Phys. G **30**, S701 (2004) [arXiv:nucl-ex/0403023].

[9] J. Adams *et al.* [The STAR Collaboration], "Experimental and theoretical challenges in the search for the quark-gluon plasma: The STAR collaboration's critical assessment of the evidence from RHIC collisions", Nucl. Phys. A **757**, 102 (2005), arXiv:nucl-ex/0501009.

[10] T2K webpage – `http://jnusrv01.kek.jp/public/t2k/`

[11] J. Abraham *et al.* [Pierre Auger Collaboration], Nucl. Instrum. Meth. A **523**, 50 (2004).

[12] T. Antoni *et al.* [KASCADE Collaboration], Nucl. Instrum. Meth. A **513**, 490 (2003).

[13] K. Nakamura *et al.* (Particle Data Group), J. Phys. G 37, 075021 (2010)

[14] NA61/SHINE webpage – `http://na61.web.cern.ch/na61/xc/index.html`

[15] N. Antoniou *et al.* [NA49-future Collaboration], CERN-SPSC-2006-034, (2006)

[16] C. Strabel [for the NA61/SHINE Collaboration], "Hadro-production measurements for T2K by NA61/SHINE at the CERN SPS", arXiv:1006.0767v1 [hep-ex].

[17] T. J. Palczewski [NA61/SHINE Collaboration], "Pion Production Measurement in NA61/SHINE Experiment for High Precision Neutrino Oscillation Experiments", PoS E **PS-HEP2009** (2009) 412, arXiv:0911.2800 [hep-ex].

[18] M. Unger, for the NA61/SHINE Collaboration, "Hadron Production at Fixed Target Energies and Extensive Air Showers", [arXiv:1012.2604 [nucl-ex]].

[19] N. Abgrall [NA61 Collaboration and T2K Collaboration], "NA61-SHINE: Hadron Production Measurements for Cosmic Ray and Neutrino Experiments", arXiv:1005.3692 [hep-ex].

[20] N. Abgrall *et al.* [NA61/SHINE Collaboration], "Revised data taking schedule with ion beams", CERN-SPSC-2009-031; SPSC-P-330-ADD-5.

[21] Z. Fodor and S. D. Katz, "Critical point of QCD at finite T and mu, lattice results for physical quark masses", JHEP **0404**, 050 (2004) [arXiv:hep-lat/0402006].

[22] S. Afanasev *et al.* [NA49 Collaboration], "The NA49 large acceptance hadron detector", Nucl. Instrum. Meth. A **430**, 210 (1999).

[23] EPICS webpage – `http://www.aps.anl.gov/epics/`

[24] DSPACK webpage – `http://na49info.web.cern.ch/na49info/na49/Software/DSPACK/`

[25] K. Werner, Nucl. Phys. A525, 501c (1991);
K. Werner, Phys. Rep. 232, 87 (1993).

[26] R. Brun, F. Carminati, GEANT Detector Description and Simulation Tool, CERN Program Library Long Writeup W5013, 1993;
`http://wwwasdoc.web.cern.ch/wwwasdoc/geant/geantall.html`

[27] ROOT webpage – `http://root.cern.ch/drupal/`

[28] ROOT61 webpage – `http://na61.web.cern.ch/na61/pages/root61/`

[29] J. Podolanski and R. Armenteros, "Analysis of V-Events", Phil. Mag. 45, 13 (1954).